NASA Contractor Report 172506

NASA-CR-172506
19850010649

Inviscid Analysis of Unsteady Blade Tip Flow Correlation Studies

B.M. Rao and B. Maskew

ANALYTICAL METHODS, INC.

Redmond, WA 98052

Contract NAS1-15472

February 1985

NASA
National Aeronautics and
Space Administration

Langley Research Center
Hampton, Virginia 23665

TABLE OF CONTENTS

LIST OF FIGURES

LIST OF FIGURES (CONTINUED)

LIST OF FIGURES (CONTINUED)

LIST OF FIGURES (CONCLUDED)

LIST OF SYMBOLS

α_o	Mean angle of attack (degrees)
α_i	Amplitude of motion, mean to peak (degrees)
ω	Reduced frequency, $\frac{c}{2}\frac{f}{V_\infty}$
f	Frequency of motion (Hertz)
δt	Time-step size (seconds)
c	Blade reference chord (meters)
s	Reference semispan of blade tip (meters)
V_∞	Reference onset velocity (meters/second)
V	Local velocity (meters/second)
x,y,z	Cartesian coordinate system (meters)

C_{p_r}	Real part	Pressure coefficient divided by α_i
C_{p_i}	Imaginary Part	

1.0 INTRODUCTION

The following is the final report on the comparison of analytical and experimental pressure measurements on four oscillating helicopter rotor blade tips. Each blade tip is considered as a semispan wing oscillating in pitch about the quarter-chord axis. The four blade-tip planforms investigated include a swept, a rectangular, a tapered and an ogee shape, Figure 1.

Two computer programs, VSAERO-TS and VSAERO-H, were developed for computing the unsteady subsonic aerodynamic characteristics of arbitrarily shaped wings oscillating in pitch. both programs have a common basis (Figure 2) in program VSAERO, which is under continued development (Refs. 1 through 4) for the analysis of steady, non-linear aerodynamic characteristics of arbitrary configurations. Program VSAERO-TS is a time-stepping analysis capable of treating large amplitude motions while program VSAERO-H uses harmonic wake and small amplitude assumptions.

The basis of the computer program is a surface singularity panel method using quadrilateral panels on which doublet and source singularities are distributed in a piecewise constant form. The panel source values are directly determined by the external Neumann boundary condition controlling the normal component of the local resultant flow: the doublet values are solved after imposing the internal Dirichlet boundary condition of zero perturbation potential at the centers (underside) of all the panels simultaneously. Surface perturbation velocities are obtained from the gradient of the doublet solution, while field velocities are obtained by direct summation of all singularity panel contributions. The details of the mathematical formulation are presented in a separate theory document (5).

The program is written in standard FORTRAN IV and has been developed on the CDC Cyber 175 computer. Minor changes to the code allow it to run on an IBM 3033 computer. The time-stepping version of the unsteady code allows up to 1,000 panels (i.e., unknowns), while VSAERO-H, which uses complex variables, allows up to 240 panels. The core requirement (octal) for either program is 234 K.

The experimental results were obtained by the Institut fur Aeroelastik in the DFVLR 3 x 3 m tunnel in Gottingen, West Germany. The work was performed under an international cooperative agreement between the DFVLR and NASA.

In the following sections, the correlation between the computed and the experimental chordwise pressure distribution for the four tip shapes is presented. For the swept tip case, a complete set of cases covering the range of 0.1, 0.2 and 0.3 reduced frequencies and angles of attack of 0, 4, 8 and 12 degrees are included. Only a limited number of cases are included for the other three tip cases. The scope of the present correlation excludes the presence of extensive dynamic separation effects.

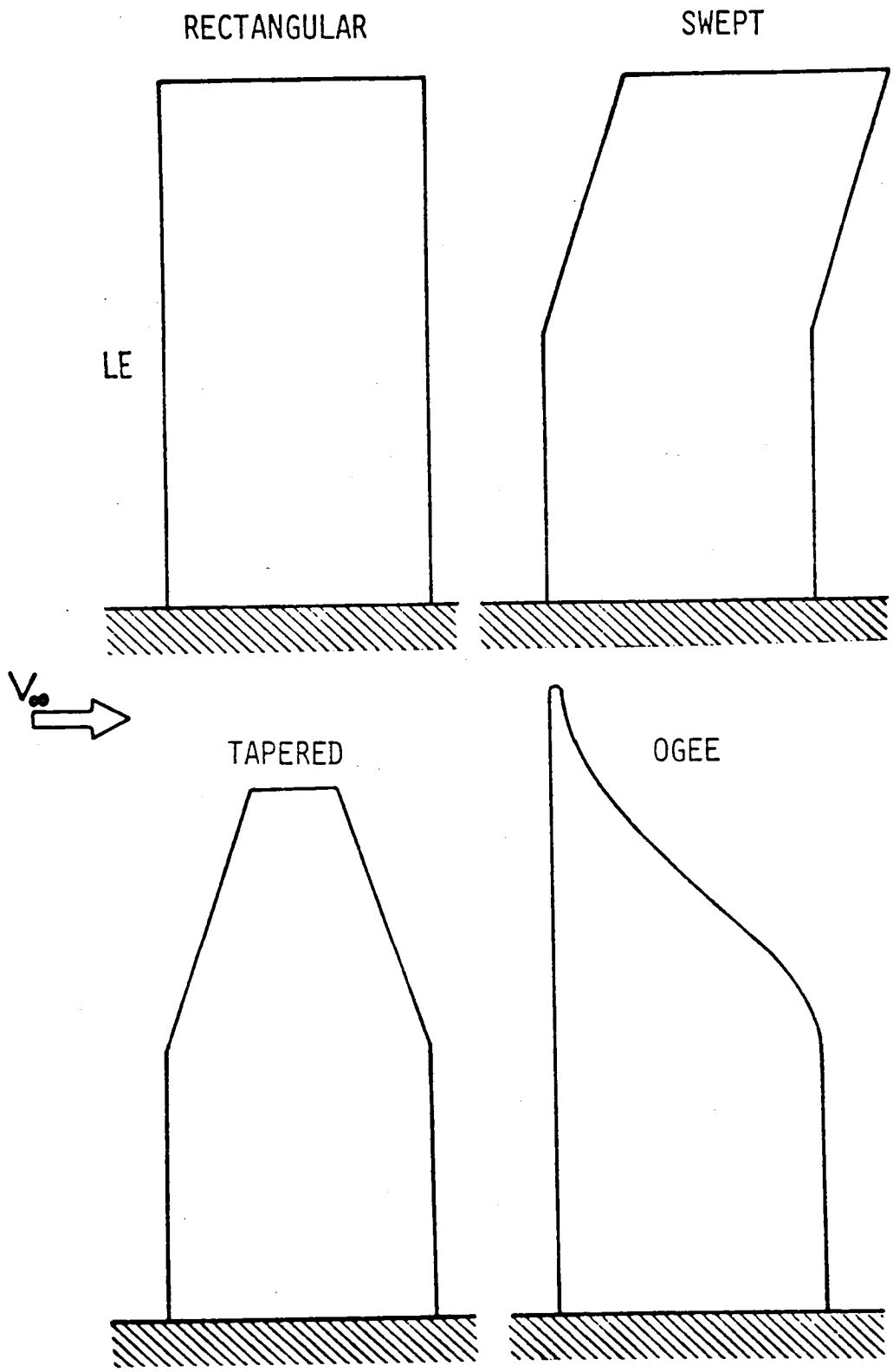

Figure 1. Planforms for Unsteady Blade Tip Study.

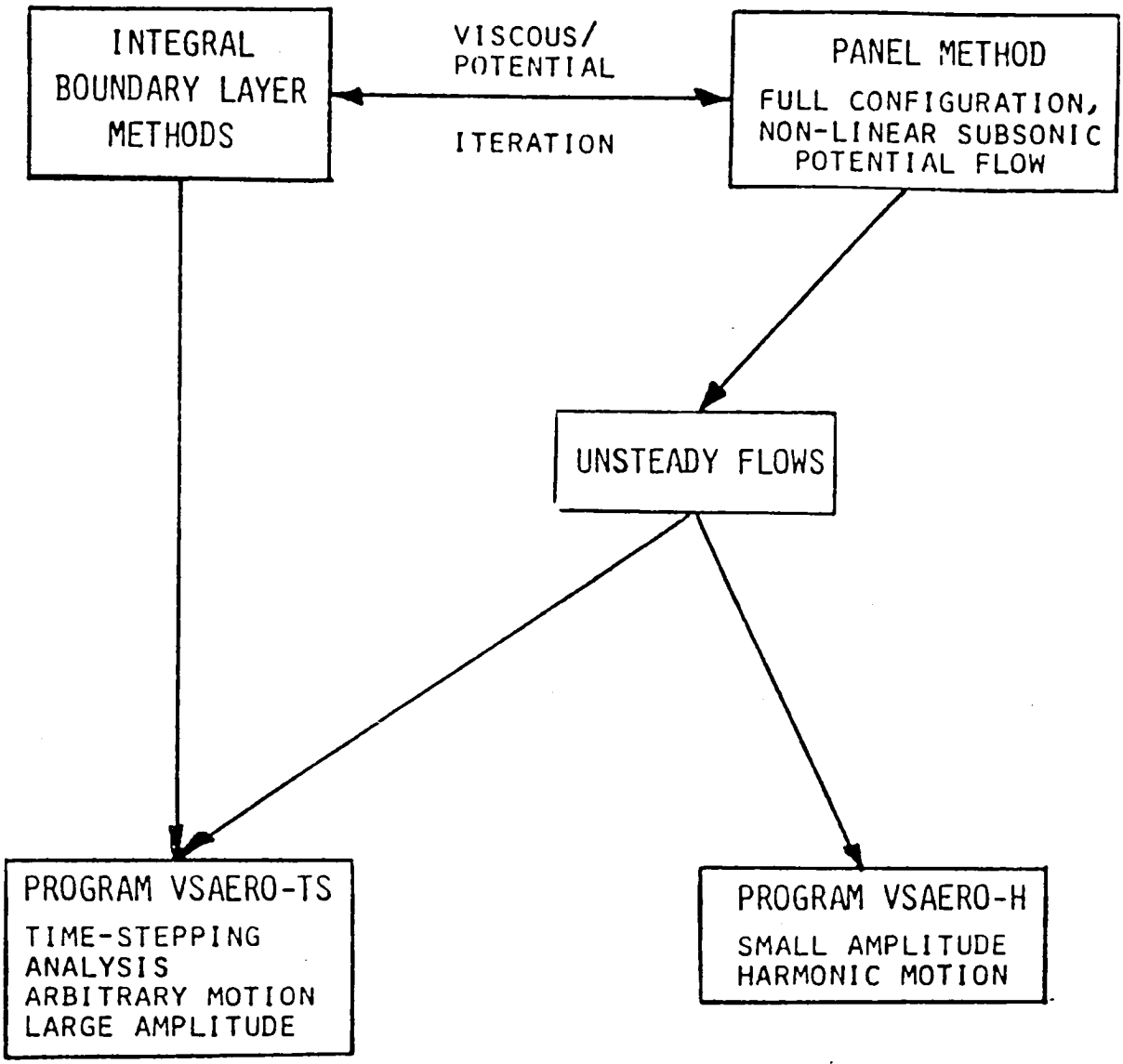

Figure 2. VSAERO Unsteady Program Development.

2.0 SWEPT TIP

VSAERO-TS is used to compute several cases for swept tip wings. The following cases of comparison between the computed and the DFVLR experimental pressure distributions are presented.

Figure No.	α_o (degrees)	α_i (degrees)	ω
3	4	0.710	0.1
4	12	0.704	0.1
5	4	0.707	0.2
6	8	0.707	0.2
7	0	0.714	0.3
8	4	0.714	0.3
9	8	0.717	0.3
10	12	0.704	0.3

Table 1. Comparison between Computed and DFVLR Experimental Pressure Distributions for the Swept Tip Wing.

The cases included in this section cover the angle of attack (mean) range of 0° to 12° and reduced frequences of 0.1, 0.2 and 0.3. For each case, the chordwise pressure distribution at the two spanwise stations, y/s = 0.48 and 0.80, between the computer (VSAERO-TS) and DFVLR tests are compared.

For the present calculations, 6 spanwise strips of panels are used; 3 up to the mid-span station (y/s = .5) where the sweep starts and 3 on the outboard section. For most of the cases run, the number of panels chordwise is 20 (10 upper and 10 lower).

The peak pressure coefficients for the real part varies from -15 to -40 as the angle of attack varies from 0° to 12°, while the peak pressures in the imaginary part are in the range $\pm$ 3. The viscous effects are not taken into account in the present calculations. (Preliminary investigations of the influence of unsteady boundary layer displacement effect on the inboard regions of the rectangular tip indicated only a small viscous correction in the range of conditions covered here.)

The correlation between calculated and experimental pressures at the outer station (y/s = .80) is very good, but this deteriorates at the inboard station (y/s = .48). The inner station is adjacent to the planform kink where the outboard sweep starts. An increase in panel density in the spanwise direction would probably improve the correlation here; however, this discrepancy does not appear for the unswept tip shapes.

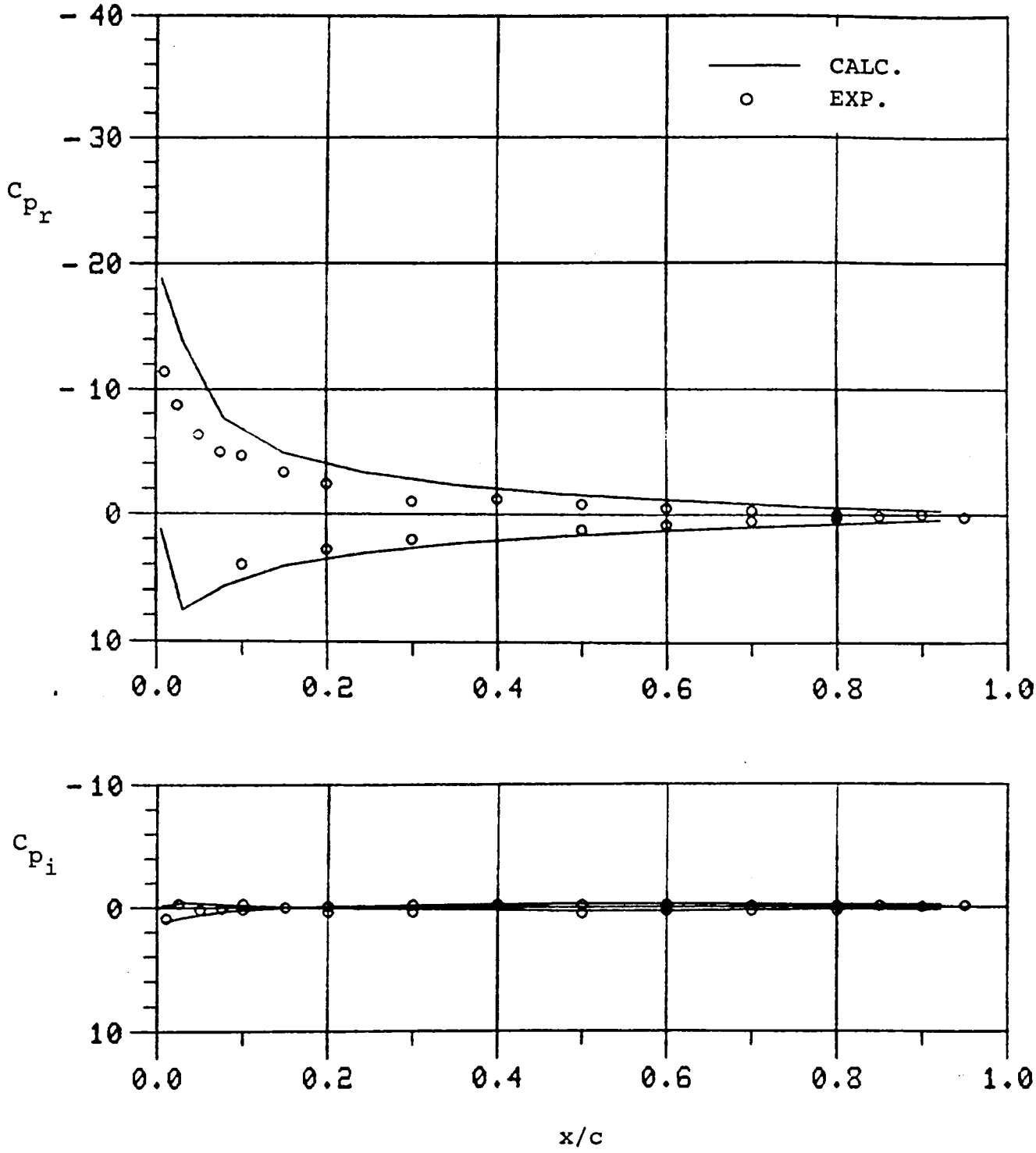

Figure 3(a). Comparison of Chordwise Pressure Distribution at y/s = 0.48 between Computed (VSAERO-TS) and DFVLR Test, Swept Tip (α_o = 4°, α_i = 0.710°, ω = 0.10).

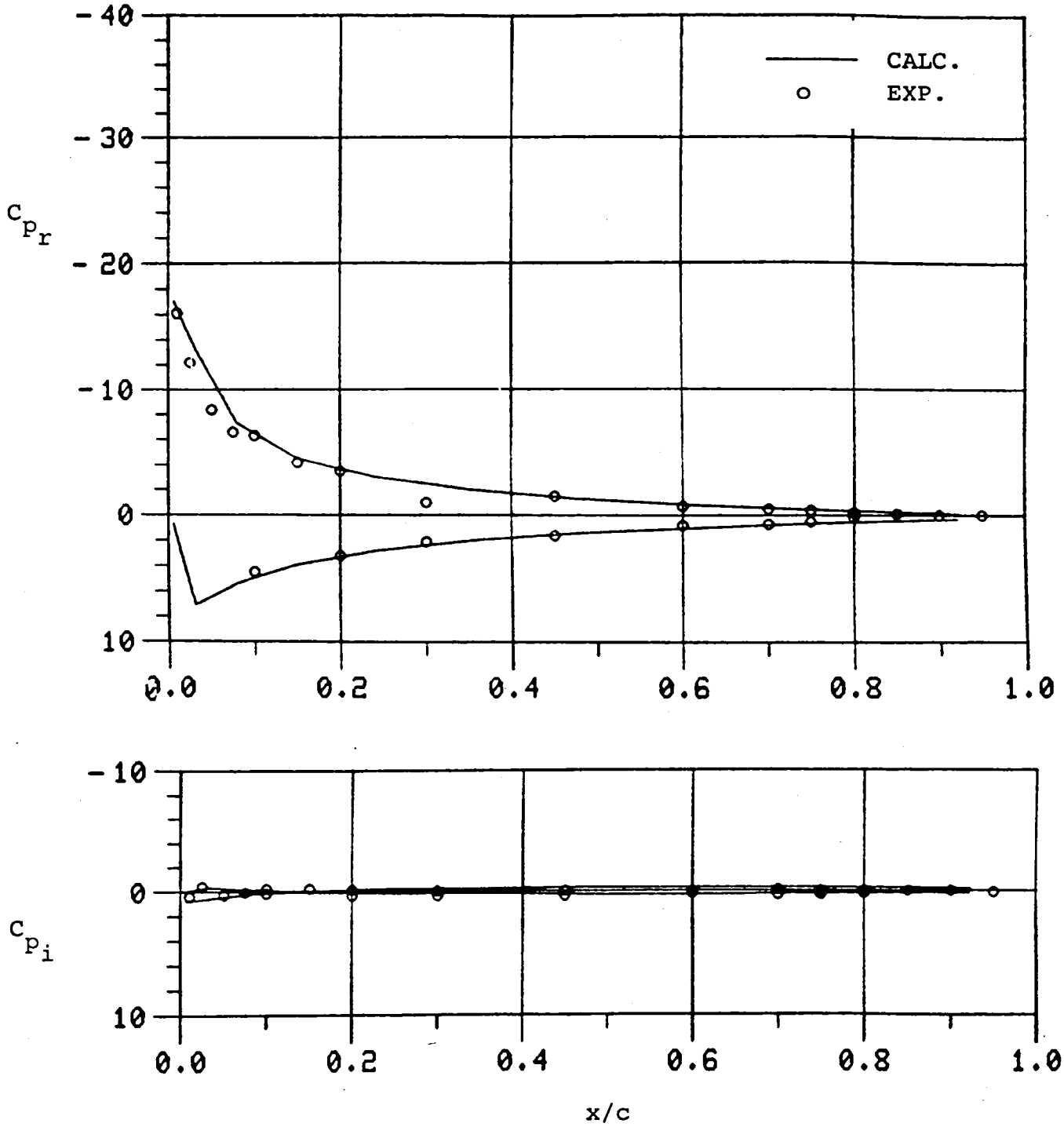

Figure 3(b). Comparison of Chordwise Pressure Distribution at y/s = 0.80 between Computed (VSAERO-TS) and DFVLR Test, Swept Tip (α_o = 4°, α_i = 0.710°, ω = 0.1).

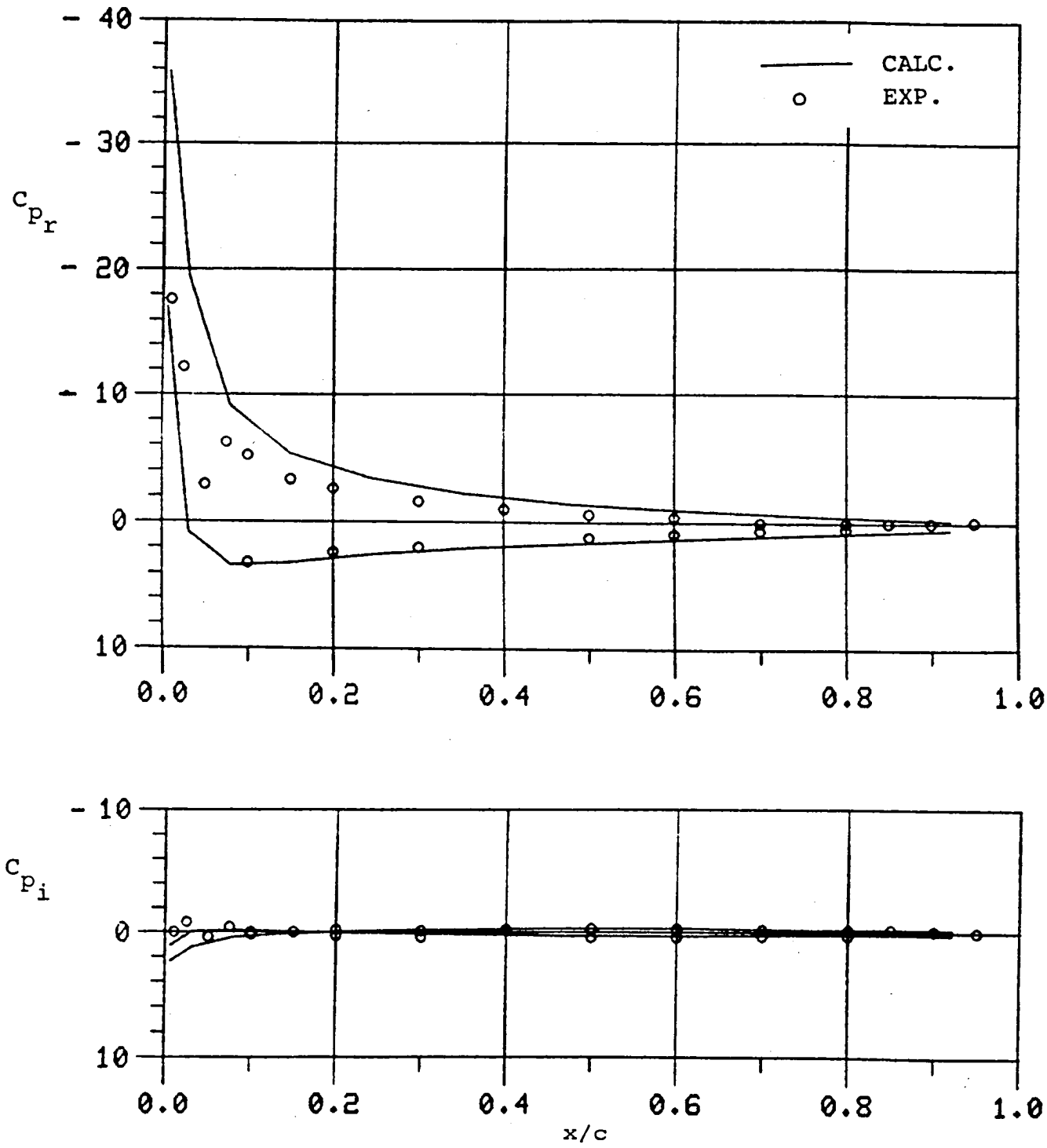

Figure 4(a).. Comparison of Chordwise Pressure Distribution at y/s = 0.48 between Computed (VSAERO-TS) and DFVLR Test, Swept Tip (α_o = 12°, α_i = 0.704°, ω = 0.1).

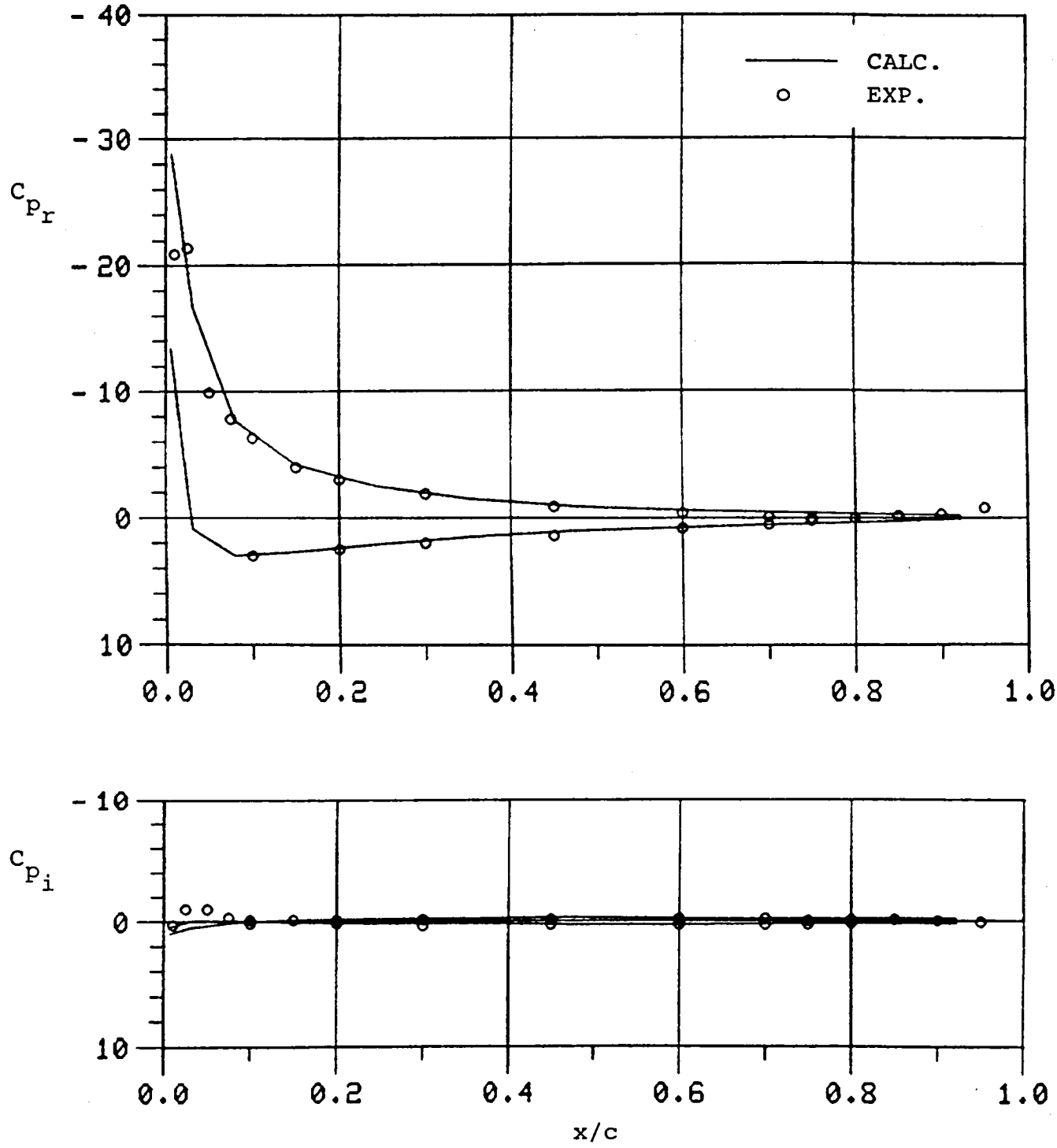

Figure 4(b). Comparison of Chordwise Pressure Distribution at y/s = 0.80 between Computed (VSAERO-TS) and DFVLR Test, Swept Tip (α_o = 12°, α_i = 0.704°, α = 0.1).

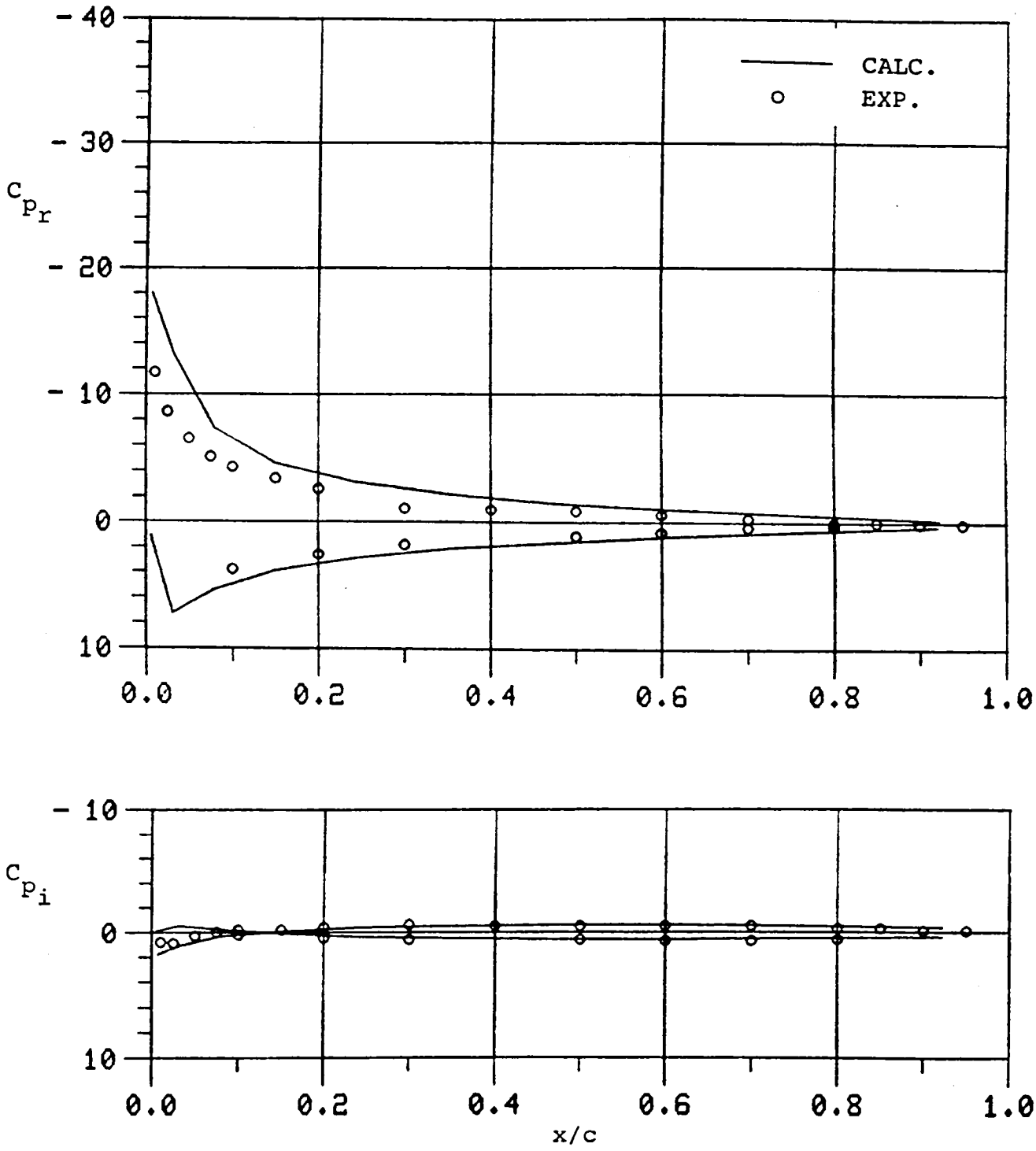

Figure 5(a). Comparison of Chordwise Pressure Distribution at y/s = 0.48 between Computed (VSAERO-TS) and DFVLR Test, Swept Tip (α_o = 4°, α_i = 0.707°, ω = 0.2).

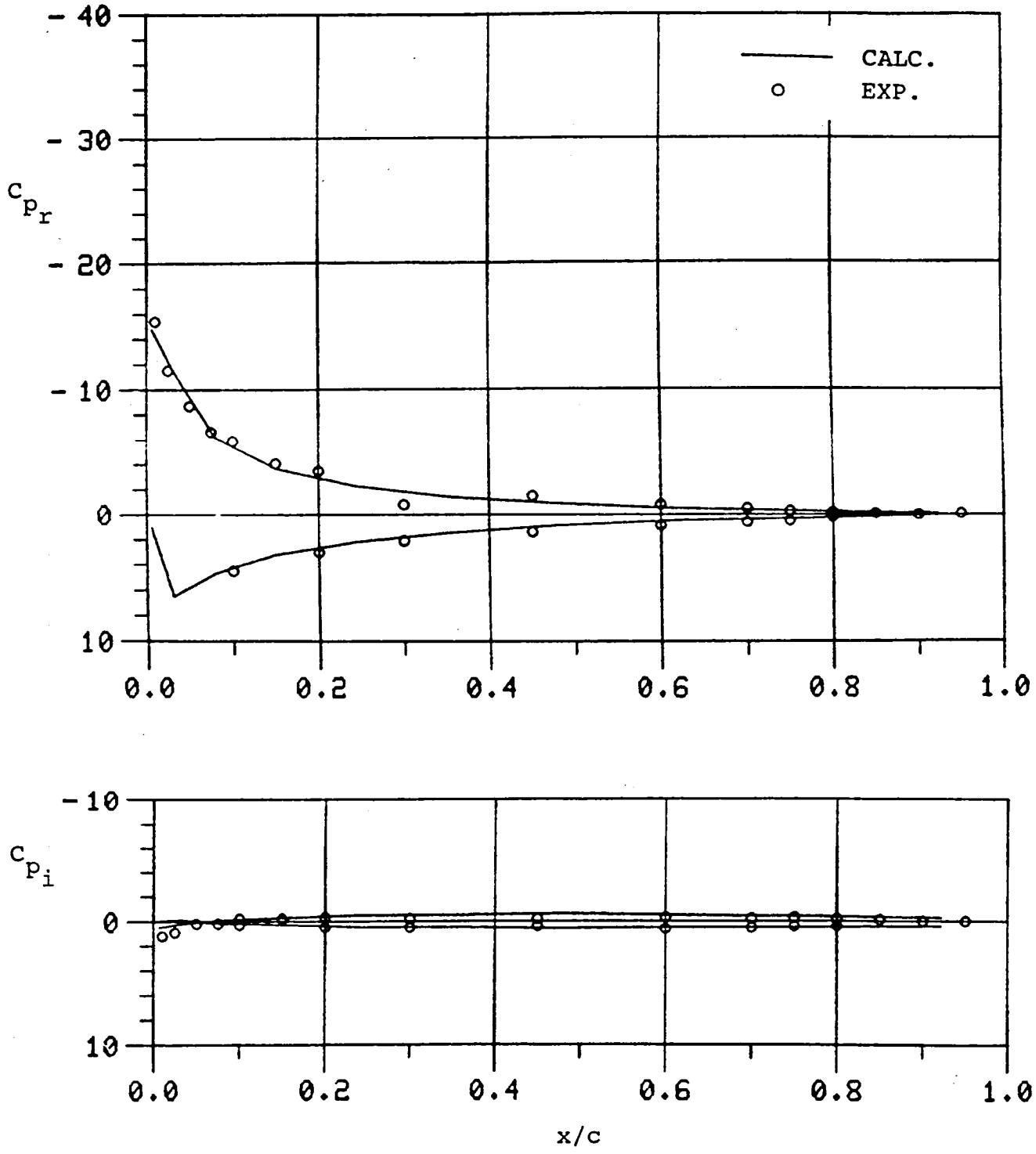

Figure 5(b). Comparison of Chordwise Pressure Distribution at y/s = 0.80 between Computed (VSAERO-TS) and DFVLR Test, Swept Tip (α_o = 4°, α_i = 0.707°, ω = 0.2).

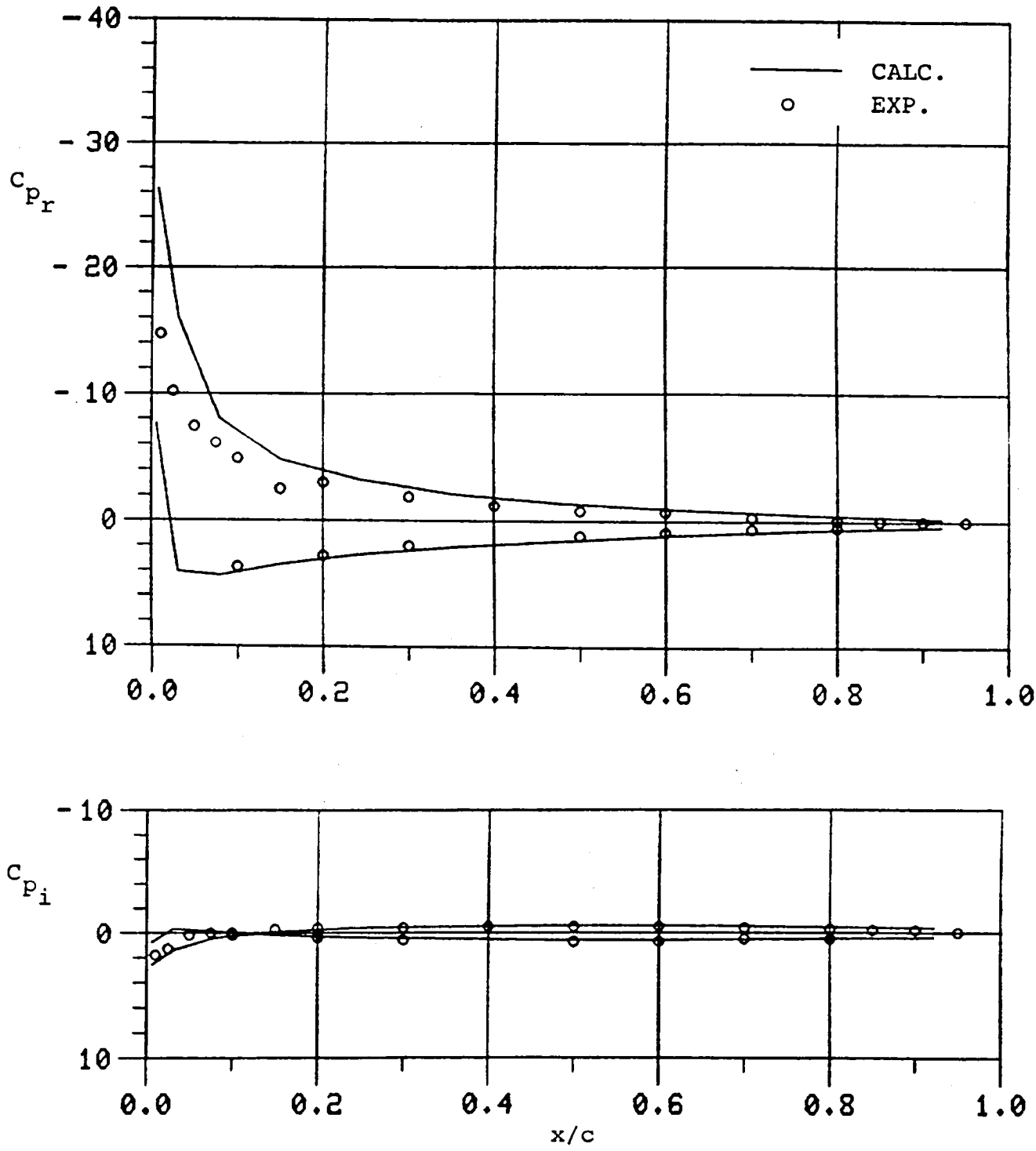

Figure 6(a). Comparison of Chordwise Pressure Distribution at y/s = 0.48 between Computed (VSAERO-TS) and DFVLR Test, Swept Tip (α_o = 8°, α_i = 0.70°, ω = 0.2).

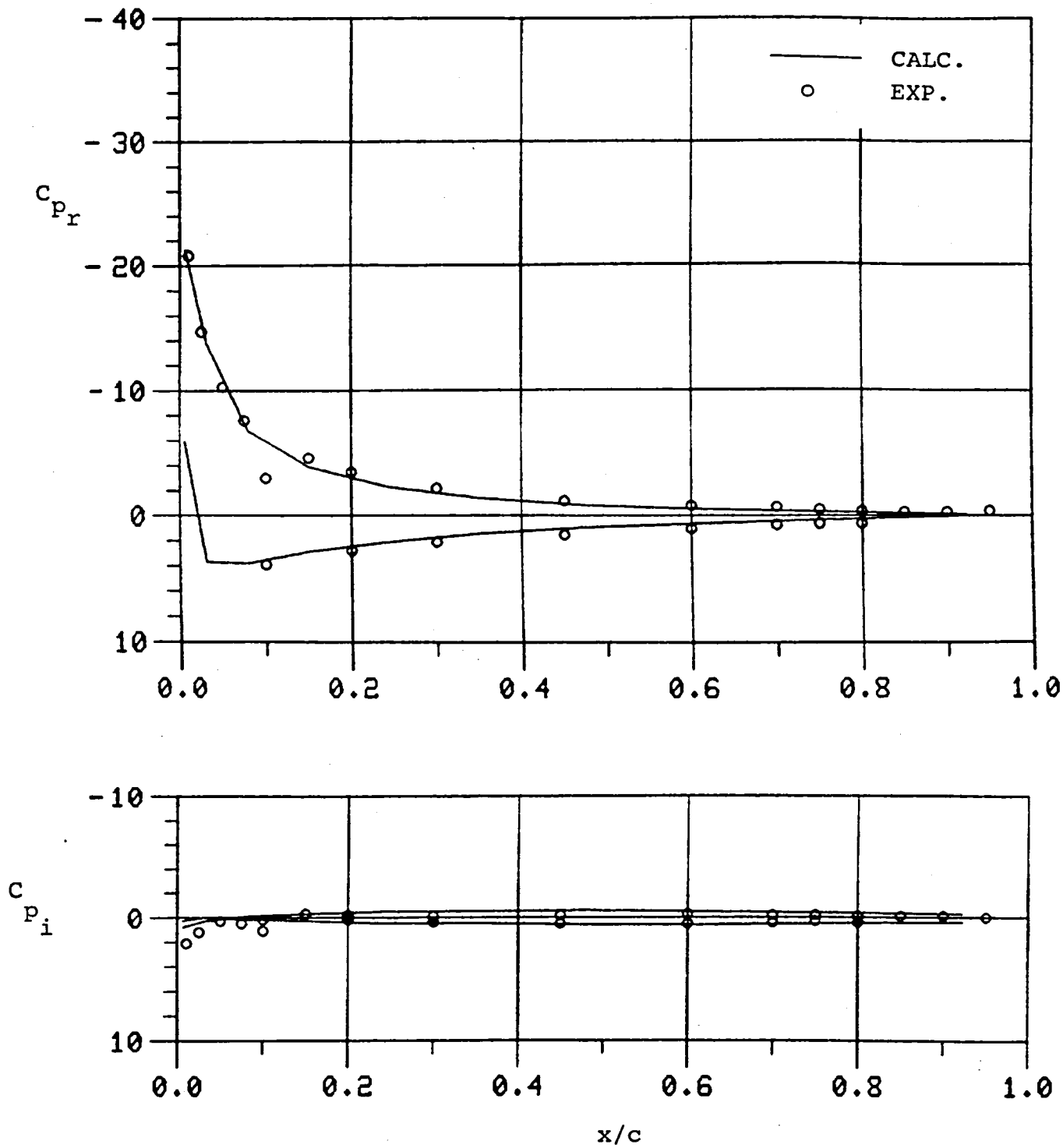

Figure 6(b). Comparison of Chordwise Pressure Distribution at y/s = 0.80 between Computed (VSAERO-TS) and DFVLR Test, Swept Tip (α_o = 8°, α_i = 0.707, ω = 0.2).

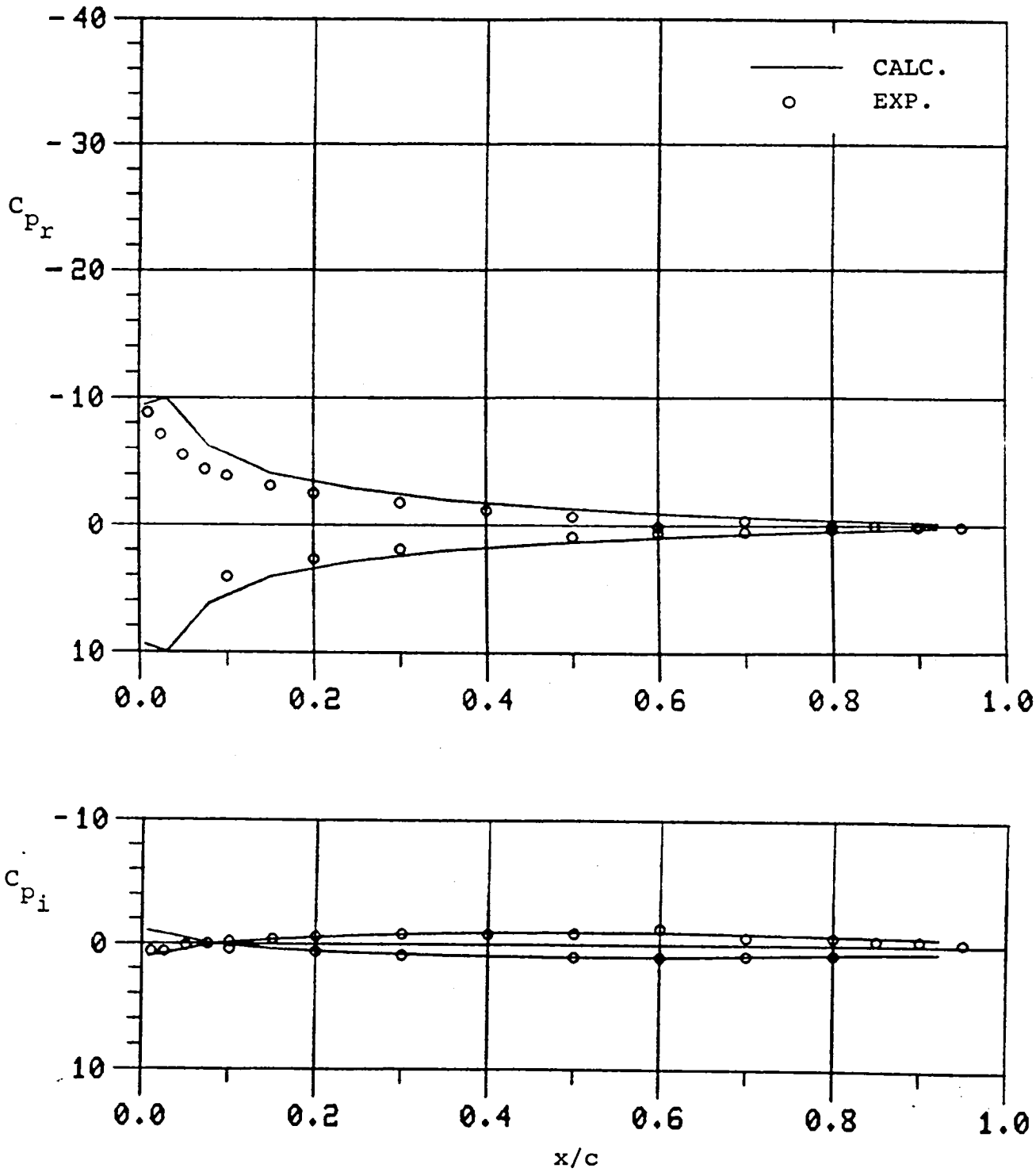

Figure 7(a). Comparison of Chordwise Pressure Distribution at y/s = 0.48 between Computed (VSAERO-TS) and DFVLR Test, Swept Tip (α_o = 0°, α_i = 0.714°, ω = 0.3).

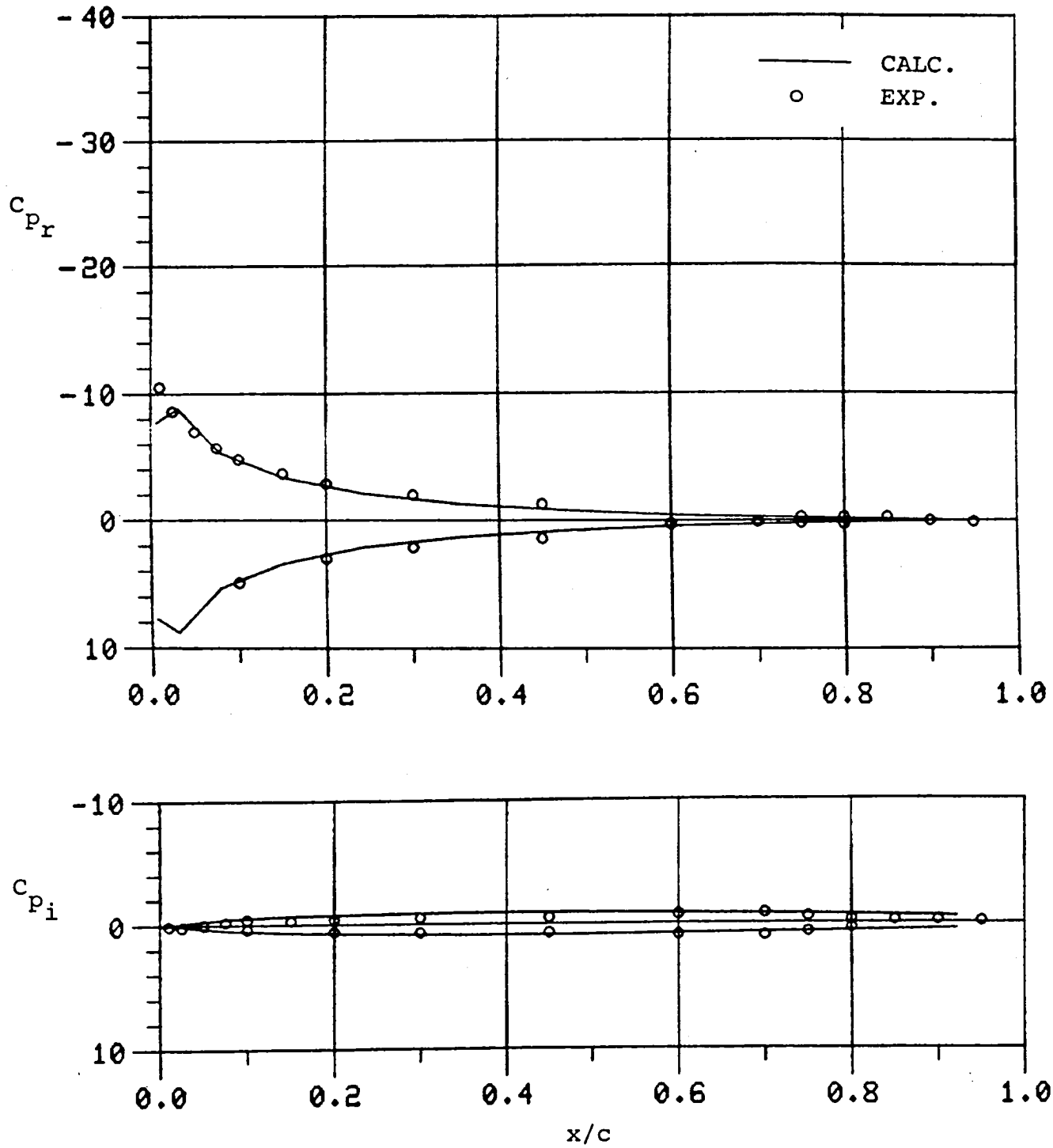

Figure 7(b). Comparison of Chordwise Pressure Distribution at y/s = 0.80 between Computed (VSAERO-TS) and DFVLR Test, Swept Tip (α_o = 0°, α_i = 0.714°, ω = 0.3).

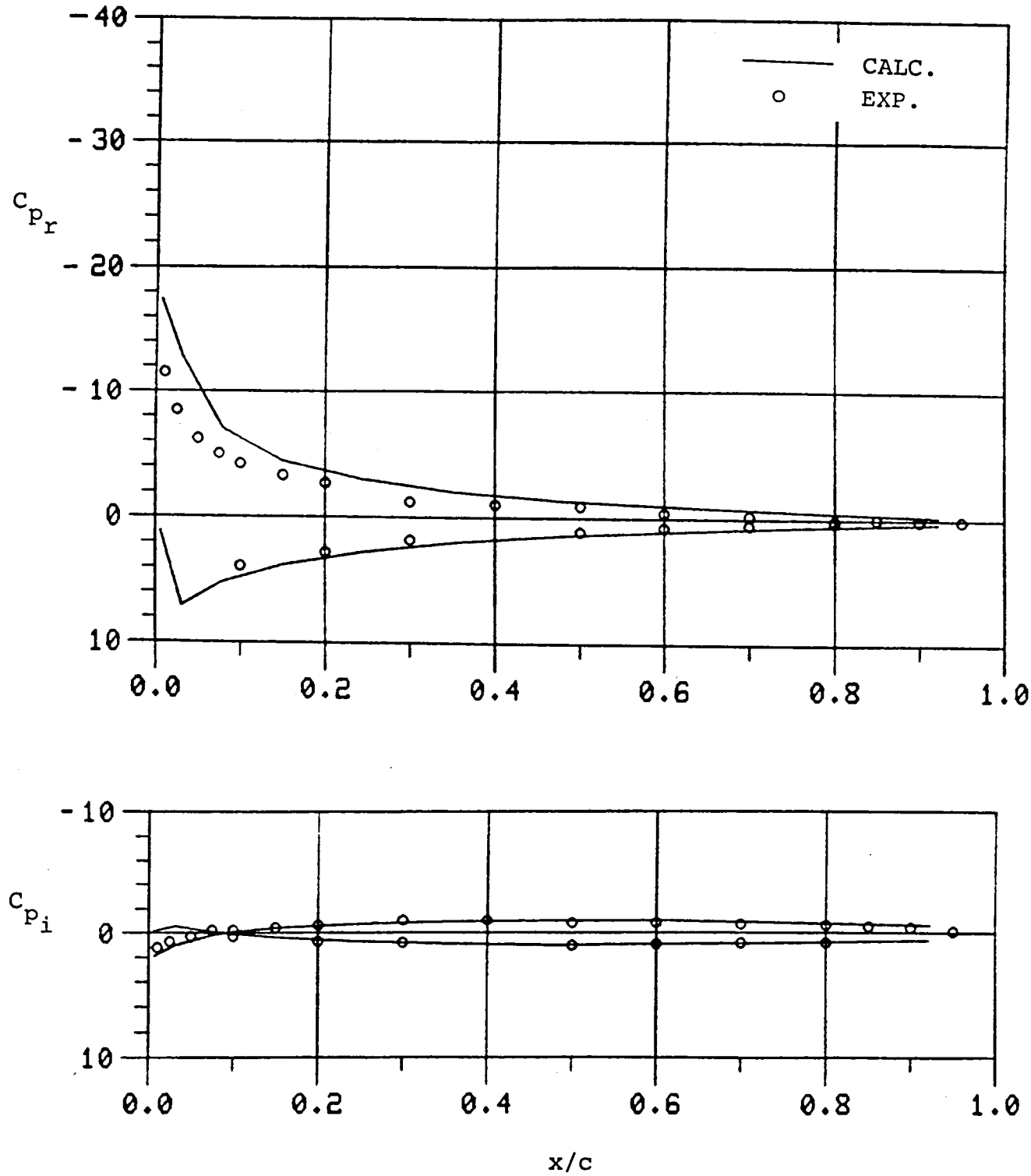

Figure 8(a). Comparison of Chordwise Pressure Distribution at y/s = 0.48 between Computed (VSAERO-TS) and DFVLR Test, Swept Tip (α_o = 4°, α_i = 0.714°, ω = 0.3).

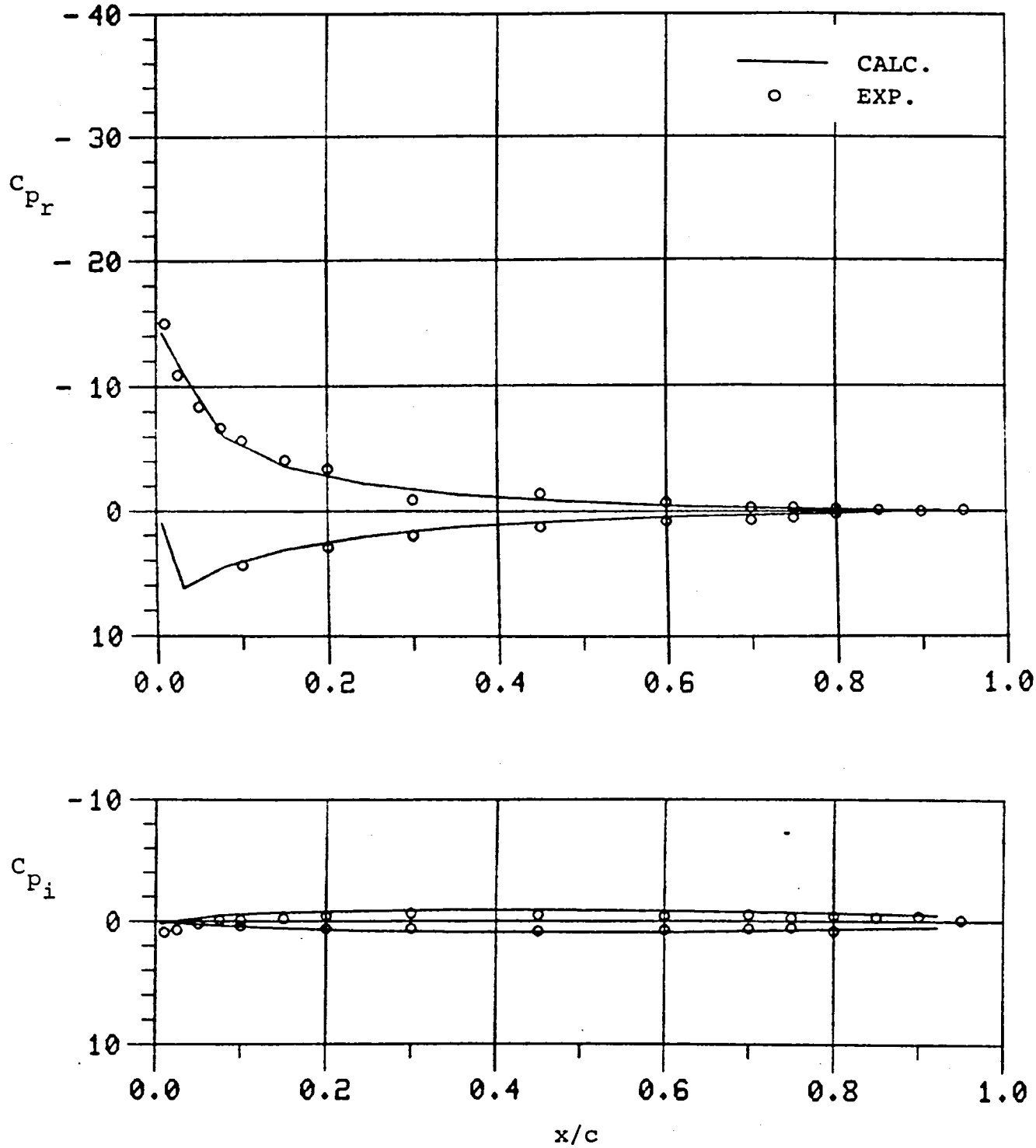

Figure 8(b). Comparison of Chordwise Pressure Distribution at y/s = 0.80 between Computed (VSAERO-TS) and DFVLR Test, Swept Tip (α_o = 4°, α_i = 0.714°, ω = 0.3).

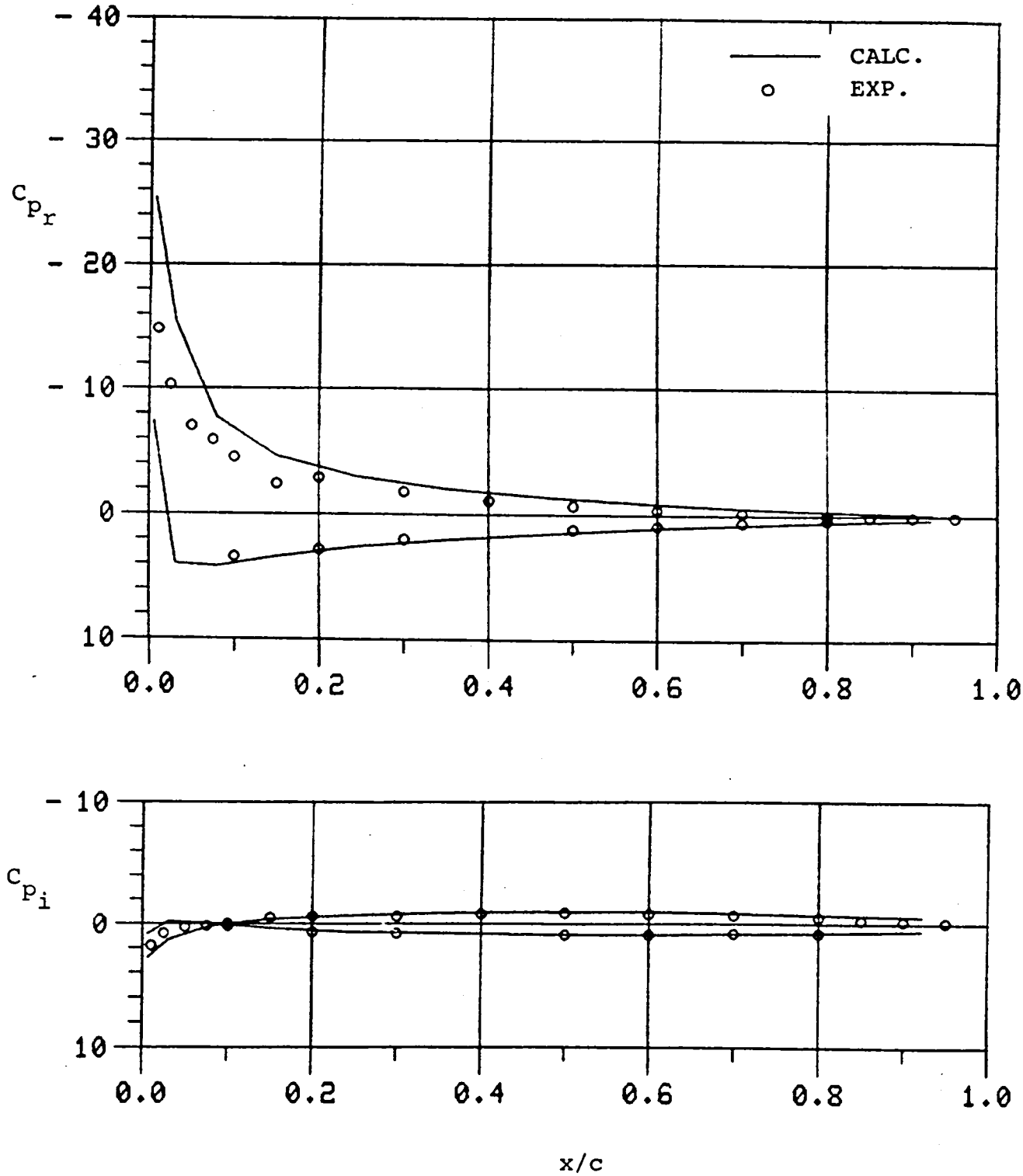

Figure 9(a). Comparison of Chordwise Pressure Distribution at y/s = 0.48 between Computed (VSAERO-TS) and DFVLR Test, Swept Tip (α_o = 8°, α_i = 0.717°, ω = 0.3).

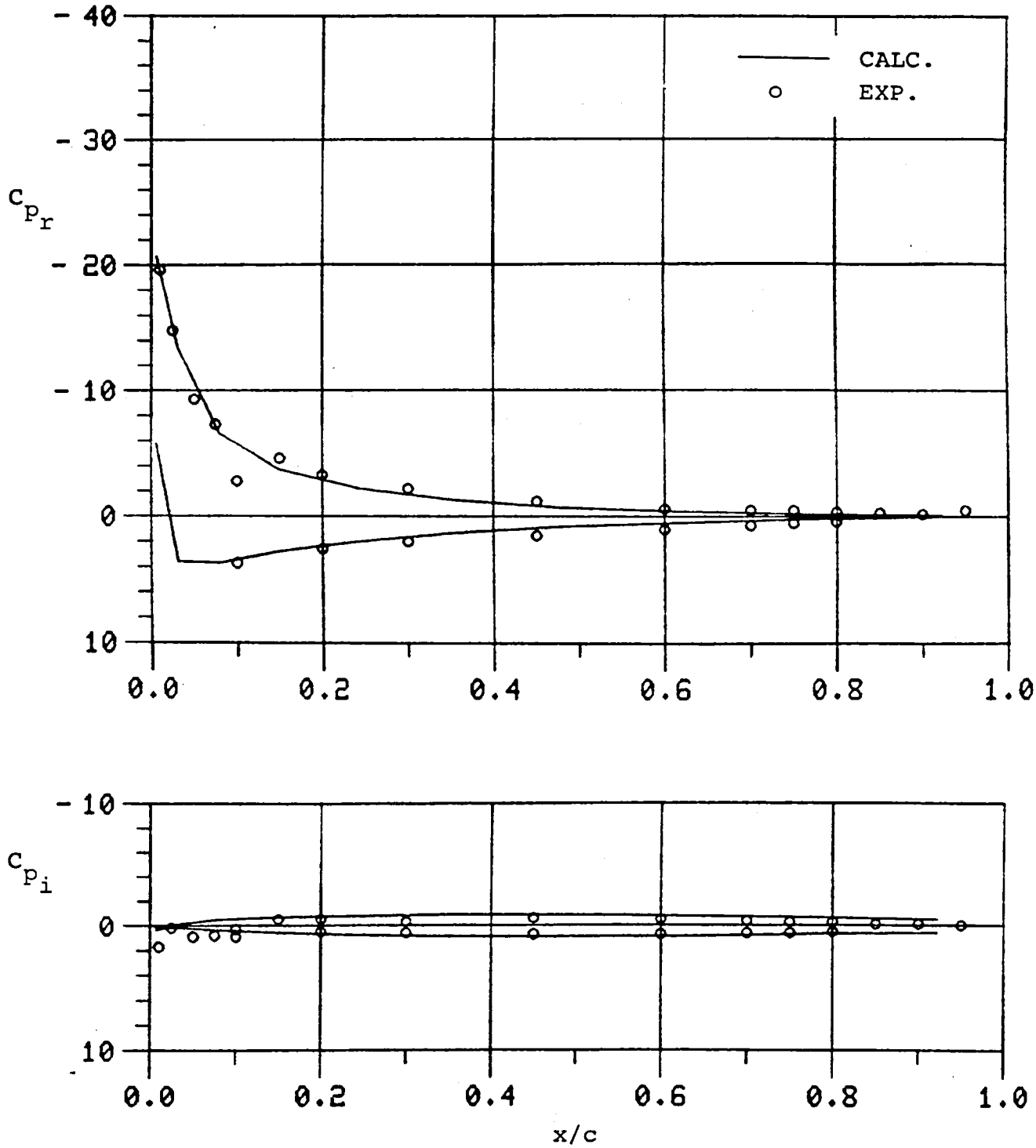

Figure 9(b). Comparison of Chordwise Pressure Distribution at y/s = 0.80 between Computed (VSAERO-TS) and DFVLR Test, Swept Tip (α_o = 8°, α_i = 0.717°, ω = 0.3).

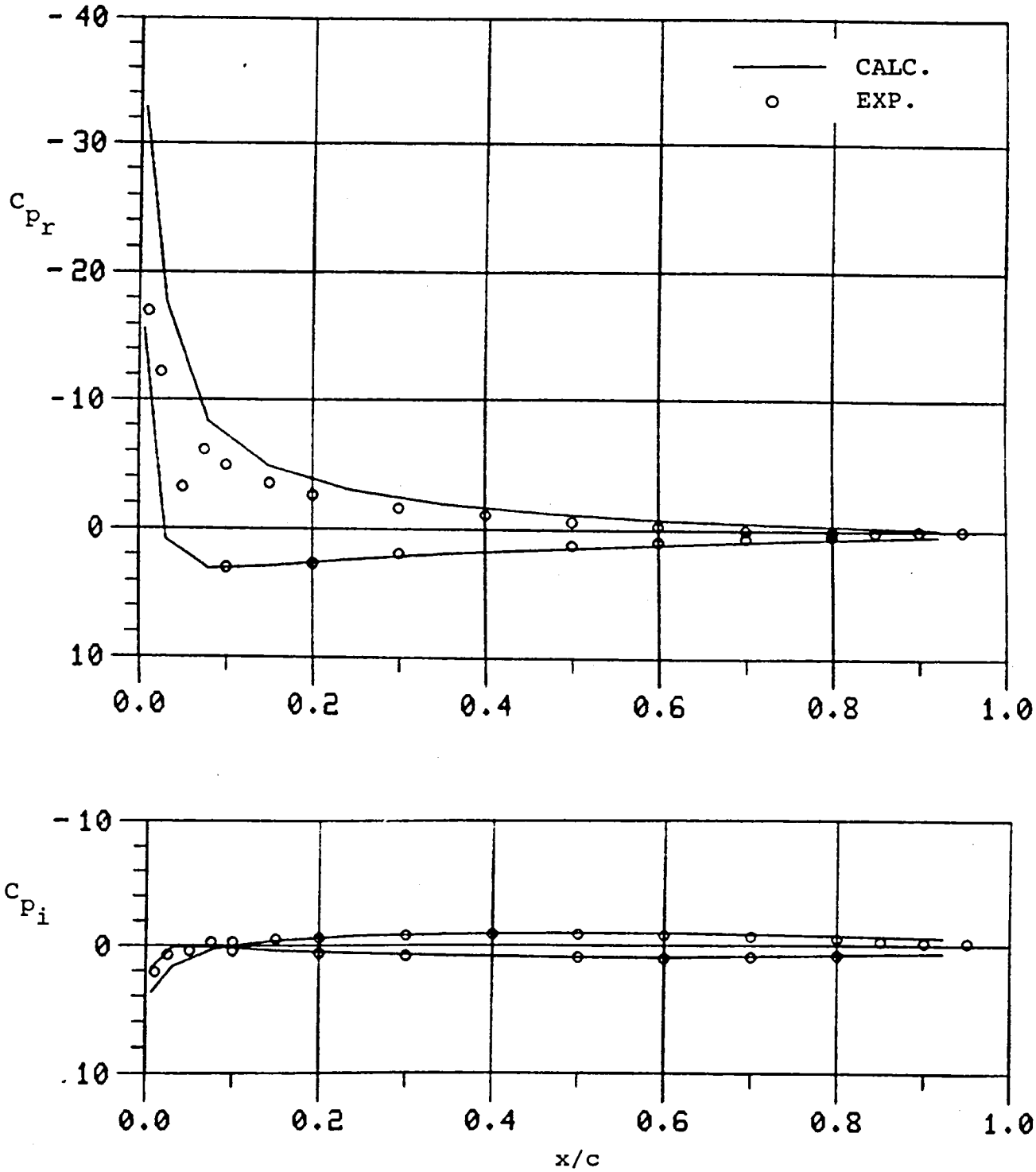

Figure 10(a). Comparison of Chordwise Pressure Distribution at y/s = 0.48 between Computed (VSAERO-TS) and DFVLR Test, Swept Tip (α_o = 12°, α_i = 0.714°, ω = 0.3).

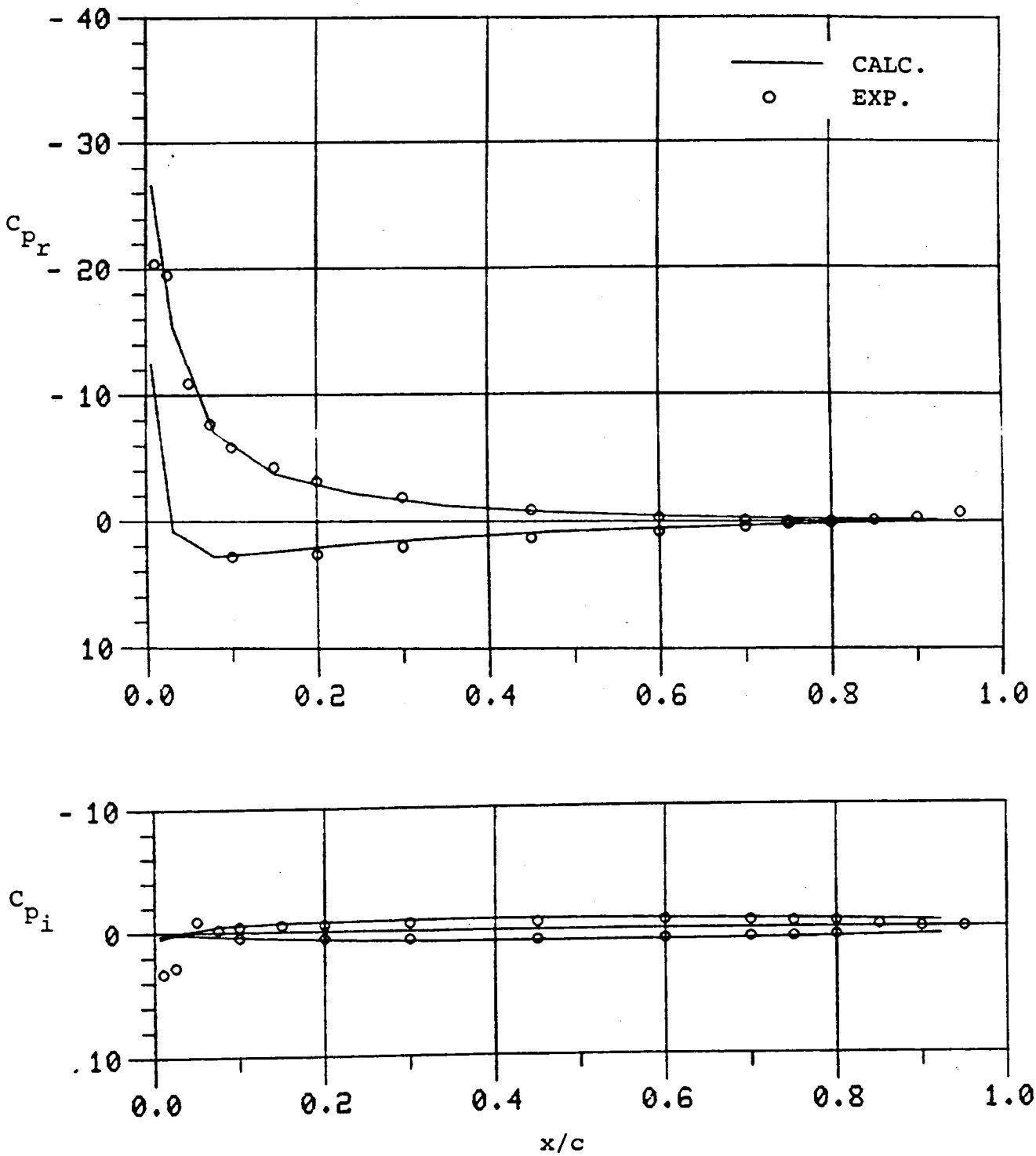

Figure 10(b). Comparison of Chordwise Pressure Distribution at y/s = 0.80 between Computed (VSAERO-TS) and DFVLR Test, Swept Tip (α_o = 12°, α_i = 0.704°, ω = 0.3).

The correlation between the computed and the experimental values, for the most part, is very good, demonstrating that VSAERO-TS is an effective computational tool for the range of angles of attack and reduced frequencies covered in this study.

The correlations are slightly better for higher frequency cases. The explanation for this is that in all these cases the same number of time steps (120 for 1 1/2 cycles) are used. For a proper comparison to the same level of computational accuracy, the number of time steps should be inversely proportional to the reduced frequency. This would maintain an essentially common step length size for the transport distance for wake elements.

3.0 RECTANGULAR TIP

A systematic parametric and sensitivity study has been conducted based on the rectangular tip case and the results are presented in a separate theory document (5). In the present document only one case is presented for this tip as the quality of the comparisons with experimental data is basically the same as for the swept tip, apart from an improvement in the semispan region.

Figure 11 shows a comparison between calculated (VSAERO-TS) and DFVLR results for the case, $\alpha_o = 12^o$, $\alpha_i = 2.066^o$, $\omega = 0.30$. The chordwise pressure distributions for real and imaginary parts are shown in Figure 11(a) through 11(d) at two spanwise stations, 0.25 semispan and 0.70 semispan. The inboard station results are representative for all four tip shapes. The correlations with the experimental data are generally very good in both the real and imaginary parts. There is, however, a tendency for the calculated imaginary pressure distributions to remain "opened out" towards the trailing edge (this is exaggerated in the present case due to the Cp scale being larger than the rest of the imaginary pressure plots). This tendency, which became more pronounced in the tip regions of the taper and ogee planforms, is probably due to an incompatibility between the size of the shedding panel and the transport distance during one time step, $V\delta t$, of points on the wake. This is discussed further in the theory document (5).

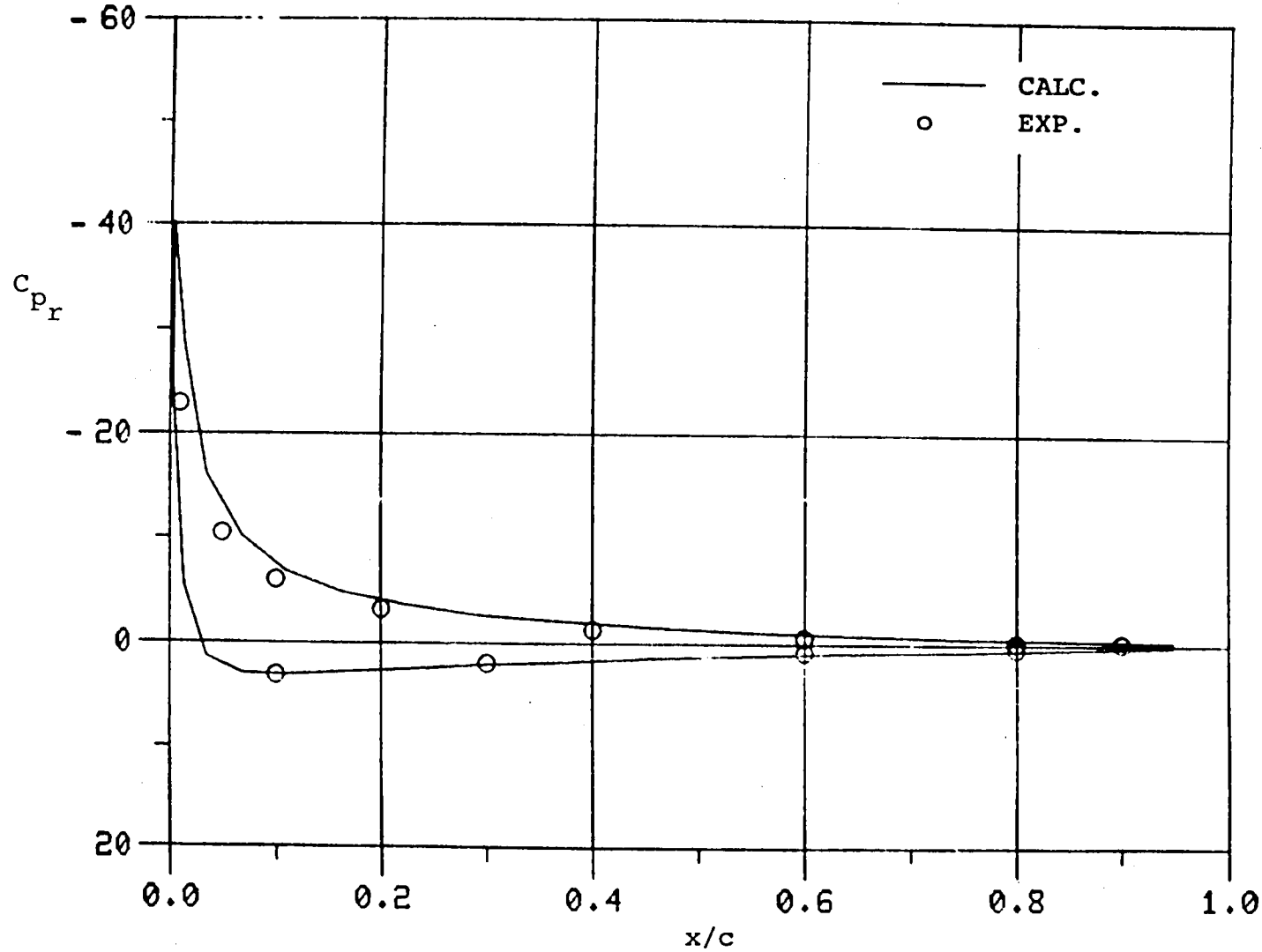

Figure 11(a). Comparison of Chordwise Pressure Distribution (Real Part) at y/s = 0.25 between Computed and DFVLR Test, Rectangular Tip (α_o = 12°, α_i = 1.066°, ω = 0.3).

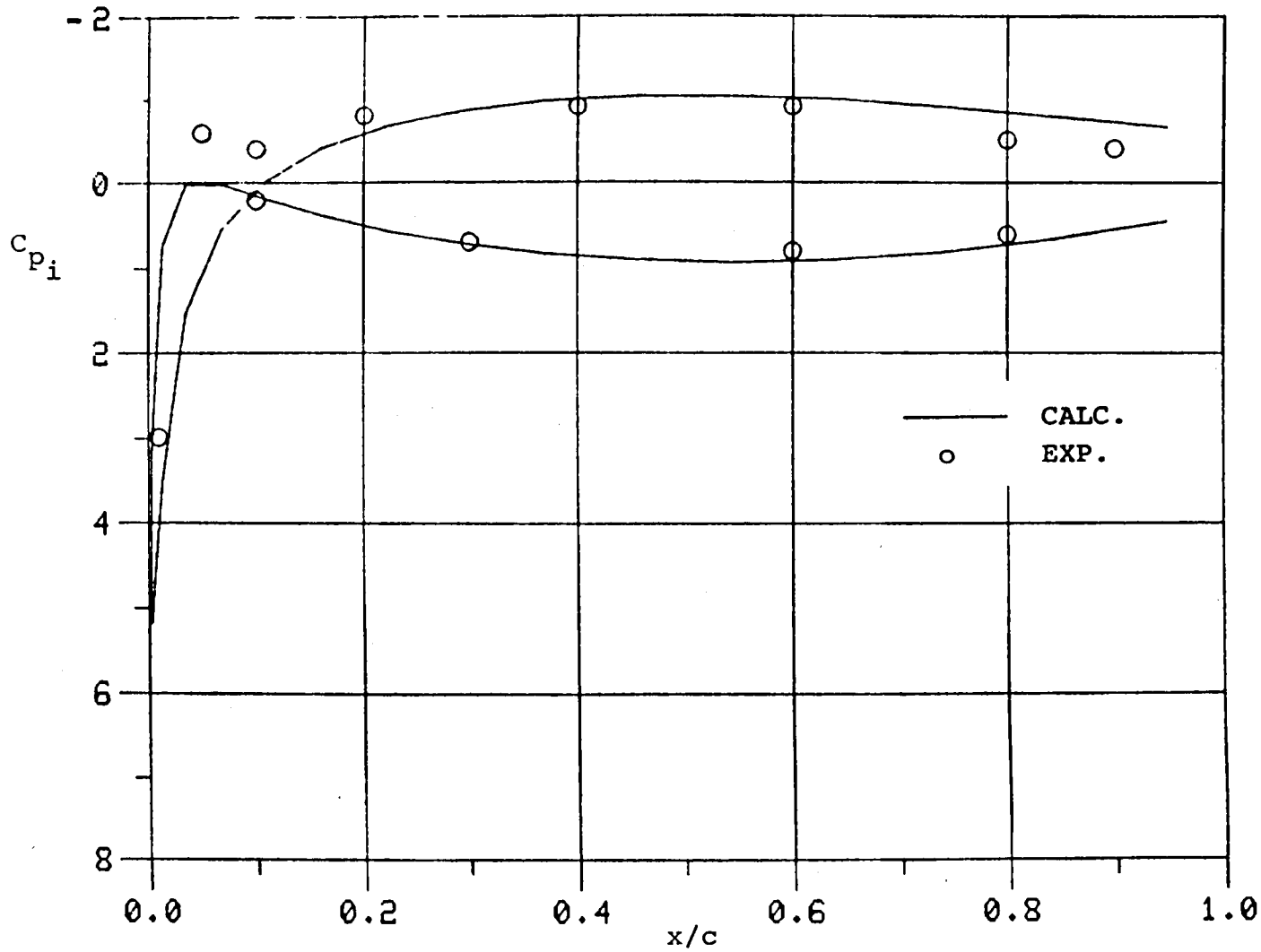

Figure 11(b). Comparison of Chordwise Pressure Distribution (Imaginary Part) at y/s = 0.25 between Computed and DFVLR Test, Rectangular Tip (α_o = 12°, α_i = 1.066°, ω = 0.3).

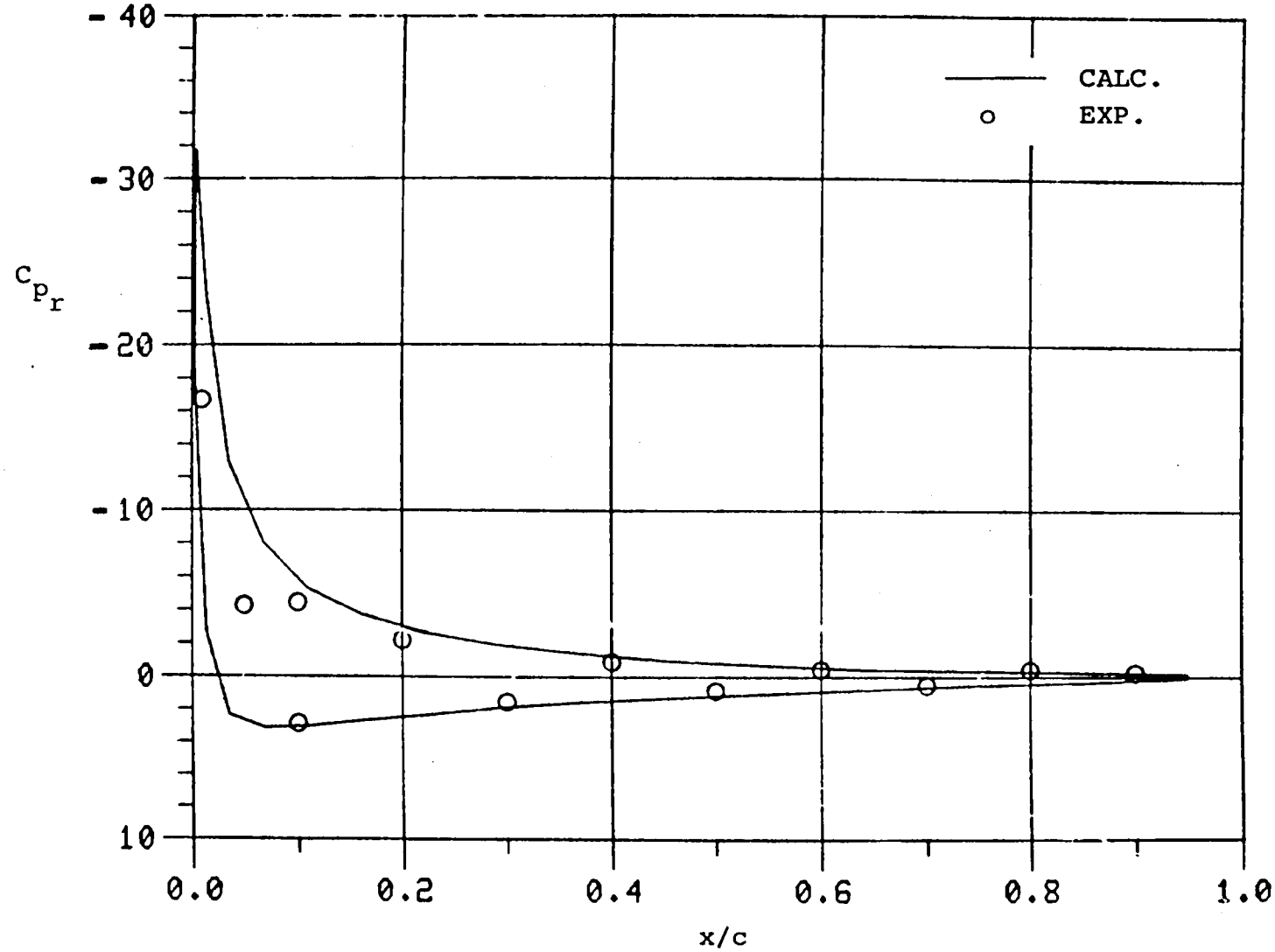

Figure 11(c). Comparison of Chordwise Pressure Distribution (Real Part) at y/s = 0.70 between Computed and DFVLR Test, Rectangular Tip (α_o = 12°, α_i = 1.066°, ω = 0.3).

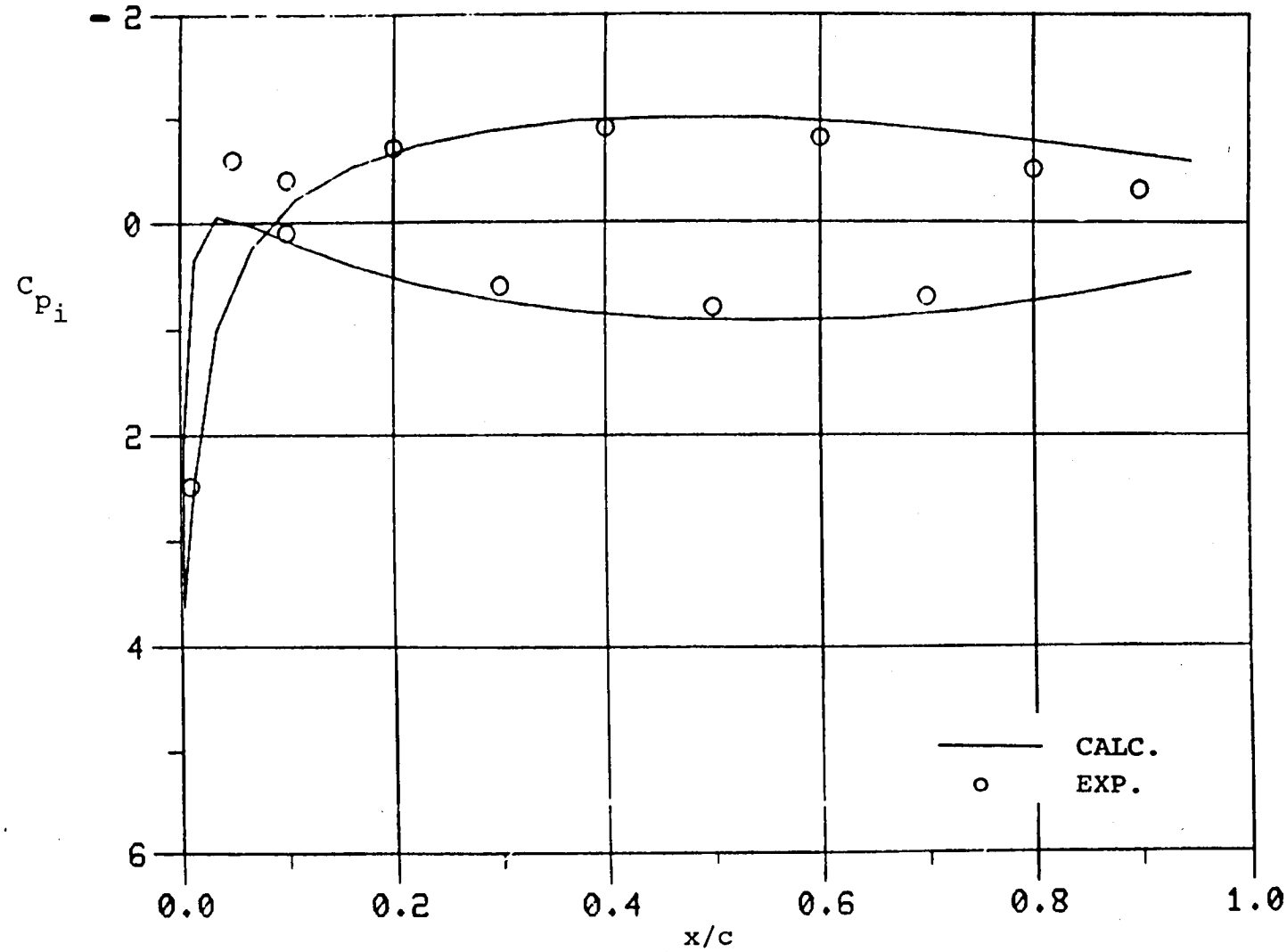

Figure 11(d). Comparison of Chordwise Pressure Distribution (Imaginary Part) at y/s = 0.70 between Computed and DFVLR Test, Rectangular Tip (α_o = 12°, α_i = 1.066°, ω = 0.3).

4.0 TAPERED TIP

VSAERO-H was used to compute several cases for the tapered tip wing. The following cases of comparison between the computed and DFVLR experimental pressure distributions are presented.

Figure No.	α_o (degrees)	α_i (degrees)	ω
12	4	0.713	0.1
13	12	0.711	0.1
14	8	0.703	0.2
15	12	0.703	0.2
16	4	0.705	0.3
17	12	0.701	0.3

Table 2. Comparison of Computed and Experimental Pressure Distributions for the Tapered Tip Wing.

The cases included in this section cover the angle of attack (steady) range of 0 to 12° and reduced frequencies of 0.1, 0.2 and 0.3. VSAERO-H was used to compute the theoretical results as VSAERO-TS required more than 120 time steps for each cycle to obtain a convergent solution in the tip region. This is due to the sensitivity of the shedding model to the relative time-step size size/shedding panel size mentioned in the previous section. This problem is discussed further in the theory document.

For each case the computed chordwise pressure distributions are compared with the DFVLR data at three spanwise stations, y/s = 0.25, 0.80 and 0.95. The comparison between the theory and experiment is good in every case except at the tip section. Since the detailed modeling of the tip vortex is not included in VSAERO-H, the discrepancy is an expected one. Although the VSAERO-TS and the DFVLR test results are not compared here for the tapered tip, the limited number of cases investigated using an impractically large number of time steps (>200) resulted in a fairly good comparison between theory and experiment.

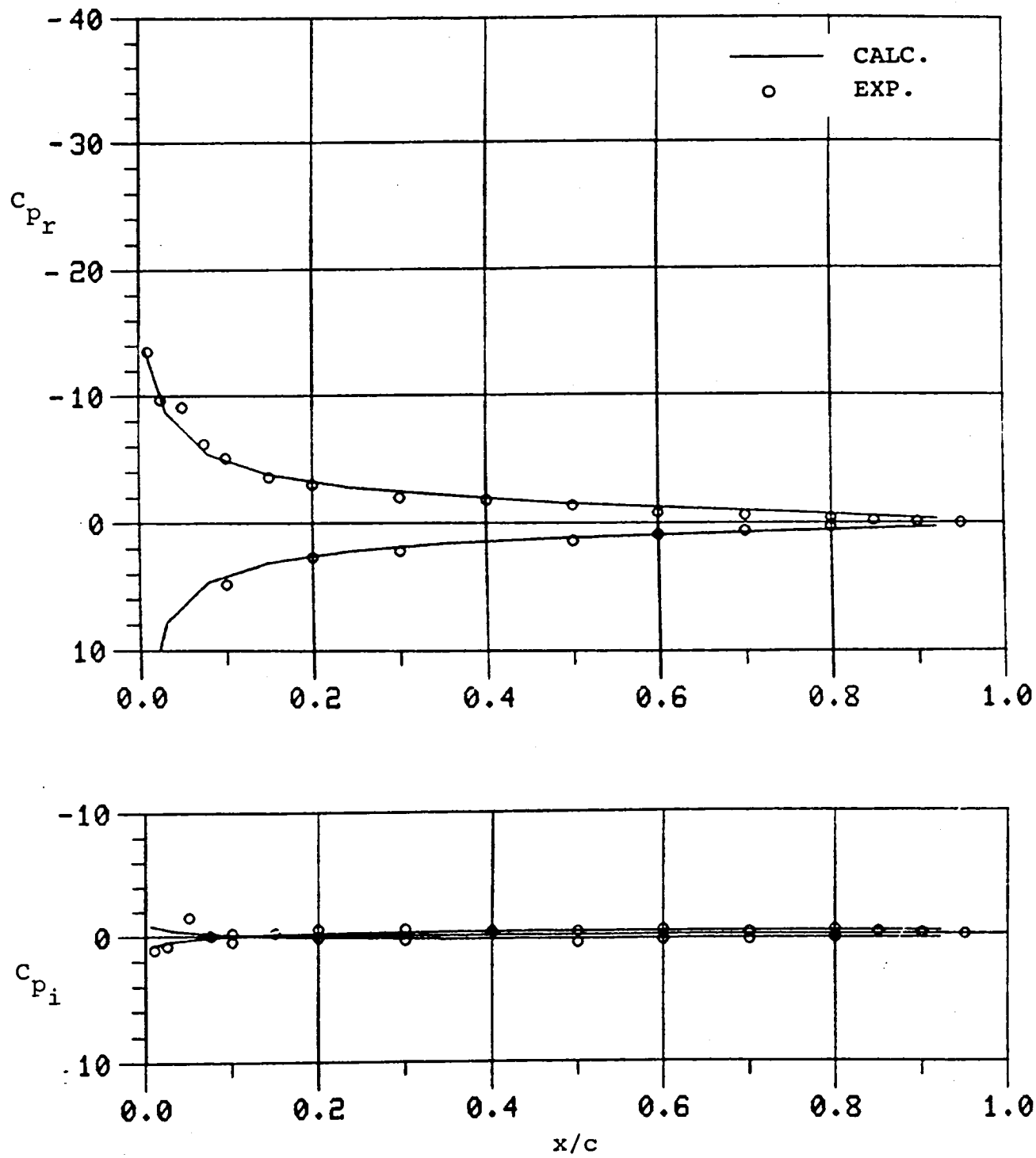

Figure 12(a). Comparison of Chordwise Pressure Distribution at y/s = 0.25 between Computed (VSAERO-H) and DFVLR Test, Tapered Tip (α_o = 4°, α_i = 0.713°, ω = 0.1).

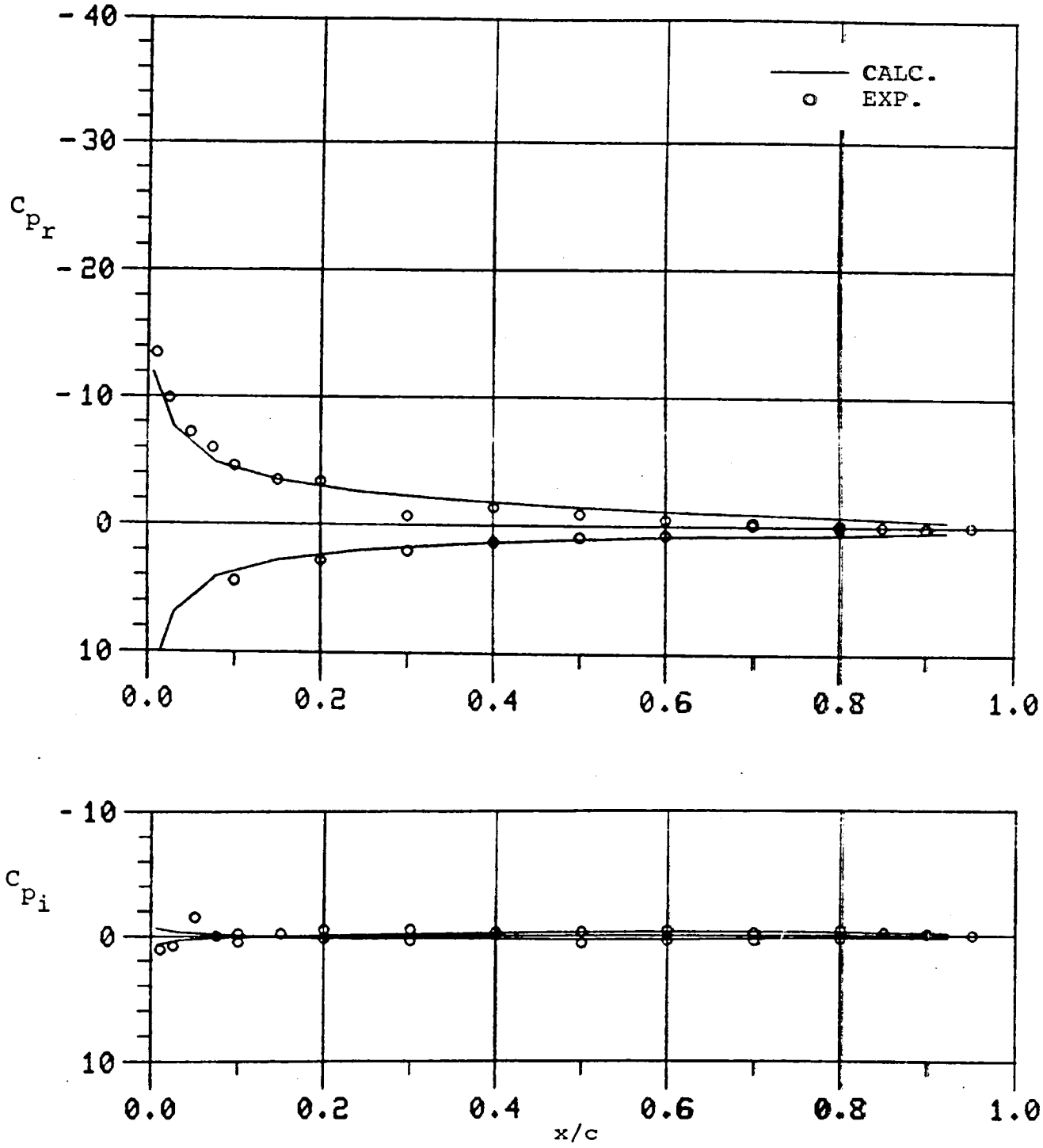

Figure 12(b). Comparison of Chordwise Pressure Distribution at y/s = 0.80 between Computed (VSAERO-H) and DFVLR Test, Tapered Tip (α_o = 4°, α_i = 0.713°, ω = 0.1).

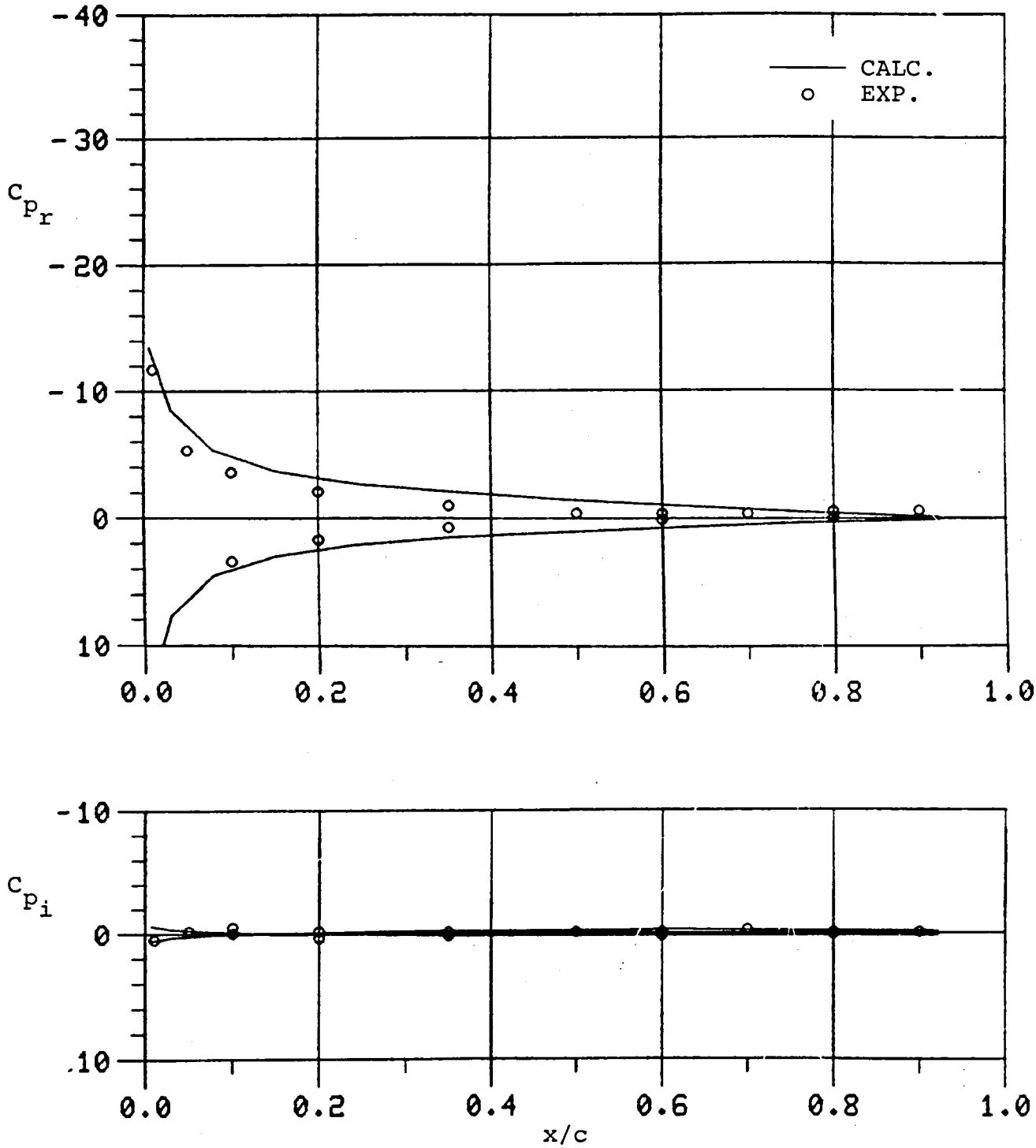

Figure 12(c). Comparison of Chordwise Pressure Distribution at y/s = 0.95 between Computed (VSAERO-H) and DFVLR Test, Tapered Tip (α_o = 4°, α_i = 0.713°, ω = 0.1).

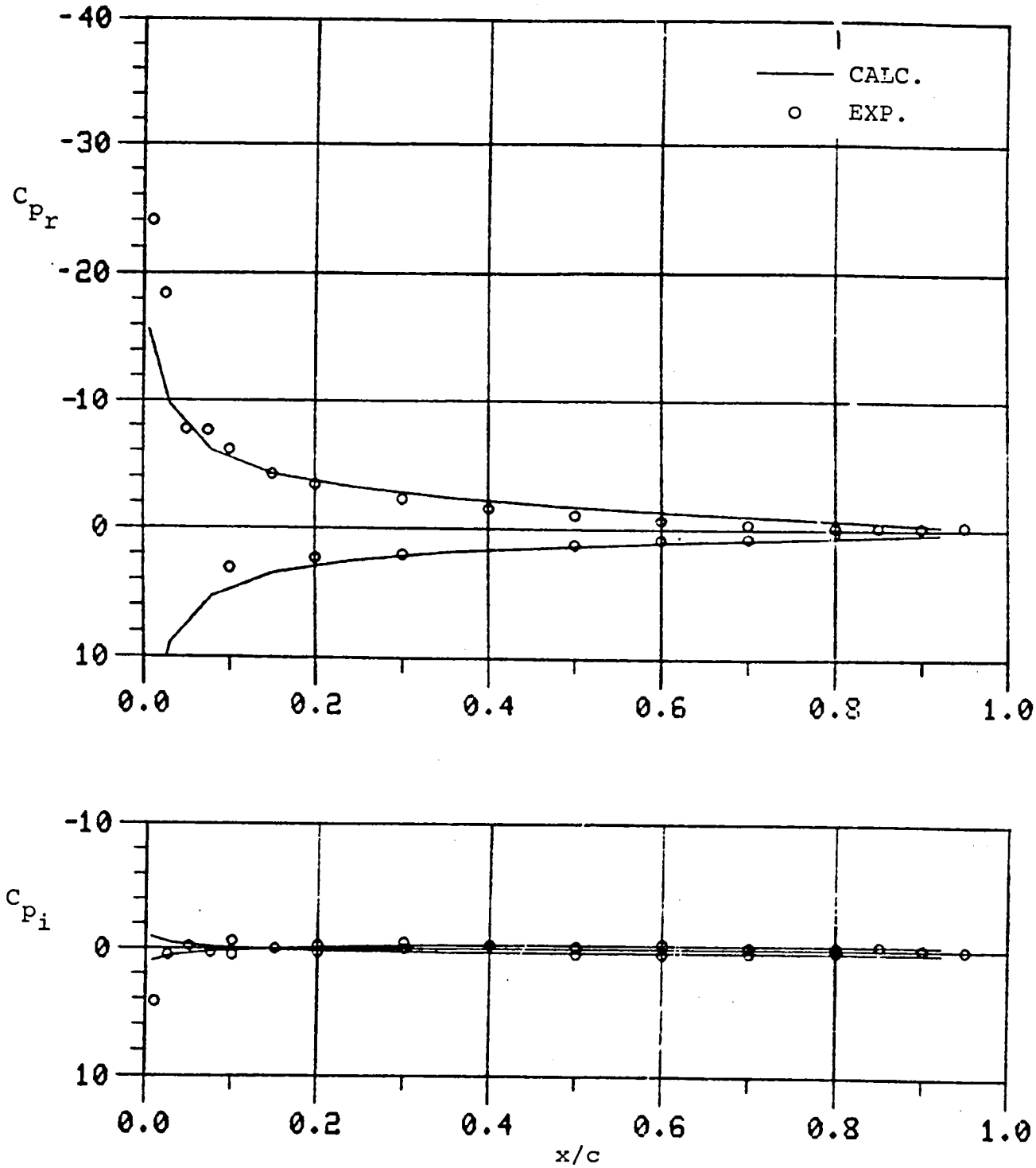

Figure 13(a). Comparison of Chordwise Pressure Distribution at y/s = 0.25 between Computed (VSAERO-H) and DFVLR Test, Tapered Tip (α_o = 12°, α_i = 0.711°, ω = 0.1).

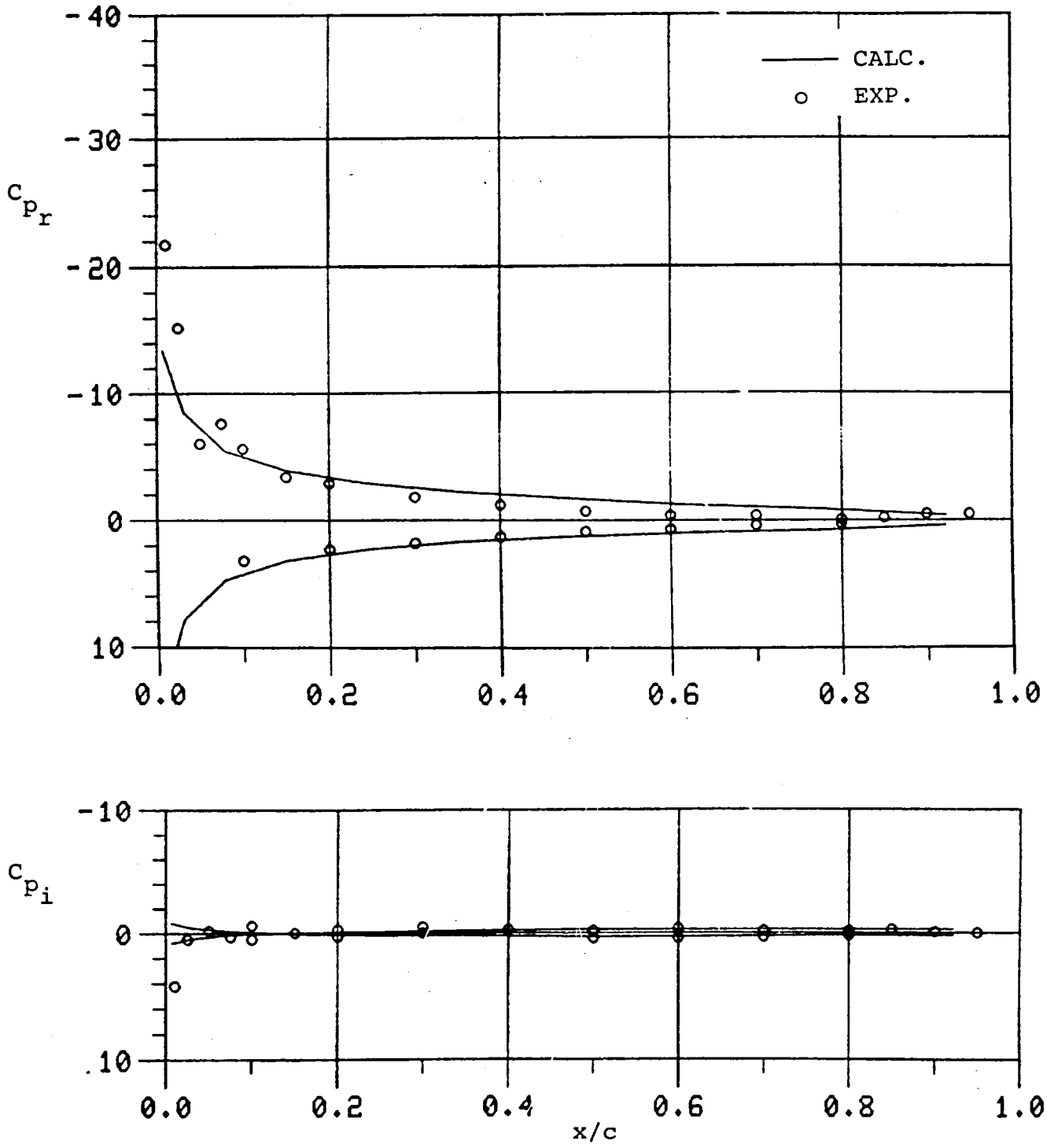

Figure 13(b). Comparison of Chordwise Pressure Distribution at y/s = 0.80 between Computed (VSAERO-H) and DFVLR Test, Tapered Tip (α_o = 12°, α_i = 0.711°, ω = 0.1).

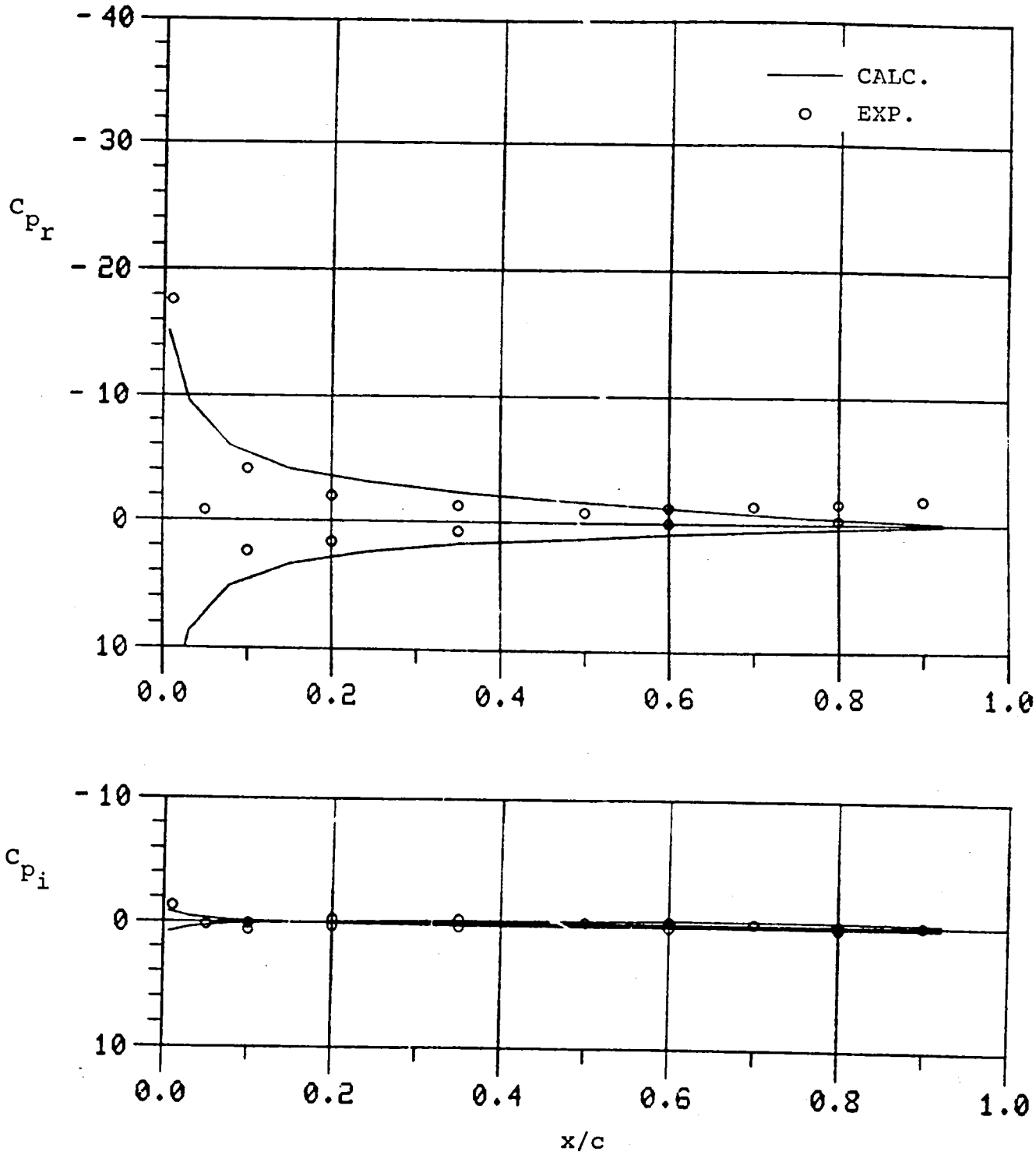

Figure 13(c). Comparison of Chordwise Pressure Distribution at y/s = 0.95 between Computed (VSAERO-H) and DFVLR Test, Tapered Tip (α_o = 12°, α_i = 0.711°, ω = 0.1).

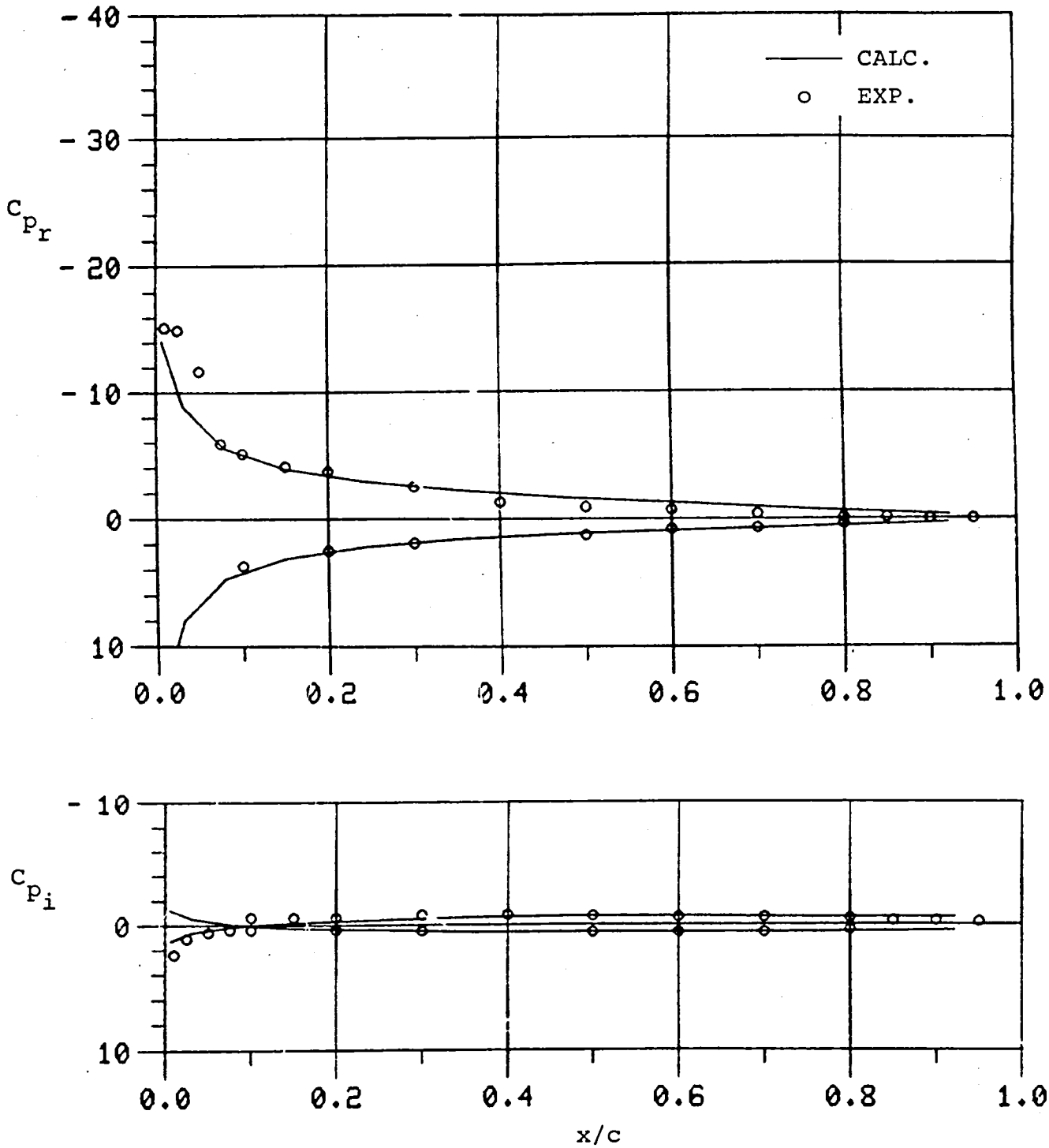

Figure 14(a). Comparison of Chordwise Pressure Distribution at y/s = 0.25 between Computed (VSAERO-H) and DFVLR Test, Tapered Tip (α_o = 8°, α_i = 0.703°, ω = 0.2).

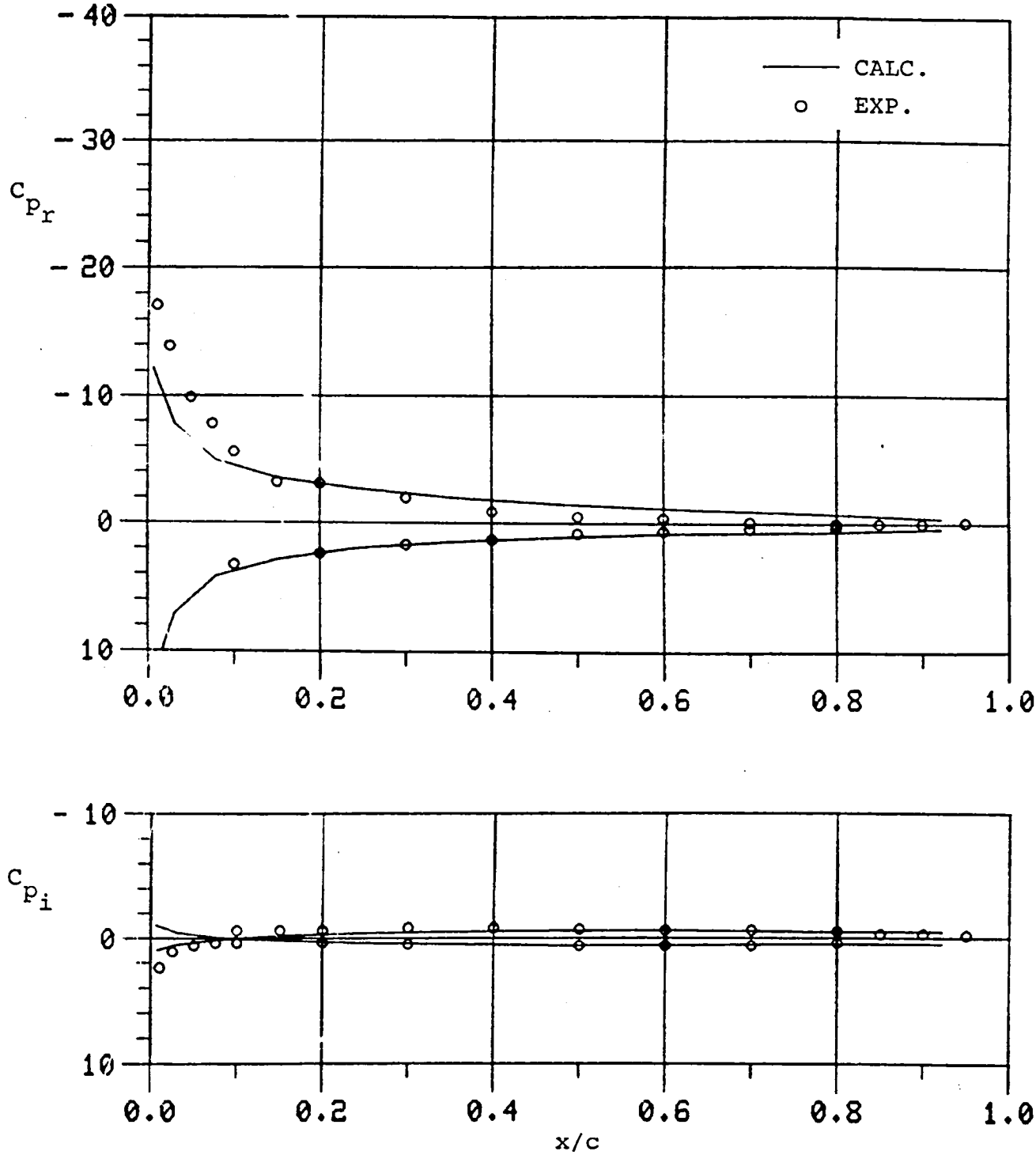

Figure 14(b). Comparison of Chordwise Pressure Distribution at y/s = 0.80 between Computer (VSAERO-H) and DFVLR Test, Tapered Tip (α_o = 8°, α_i = 0.703°, ω = 0.2).

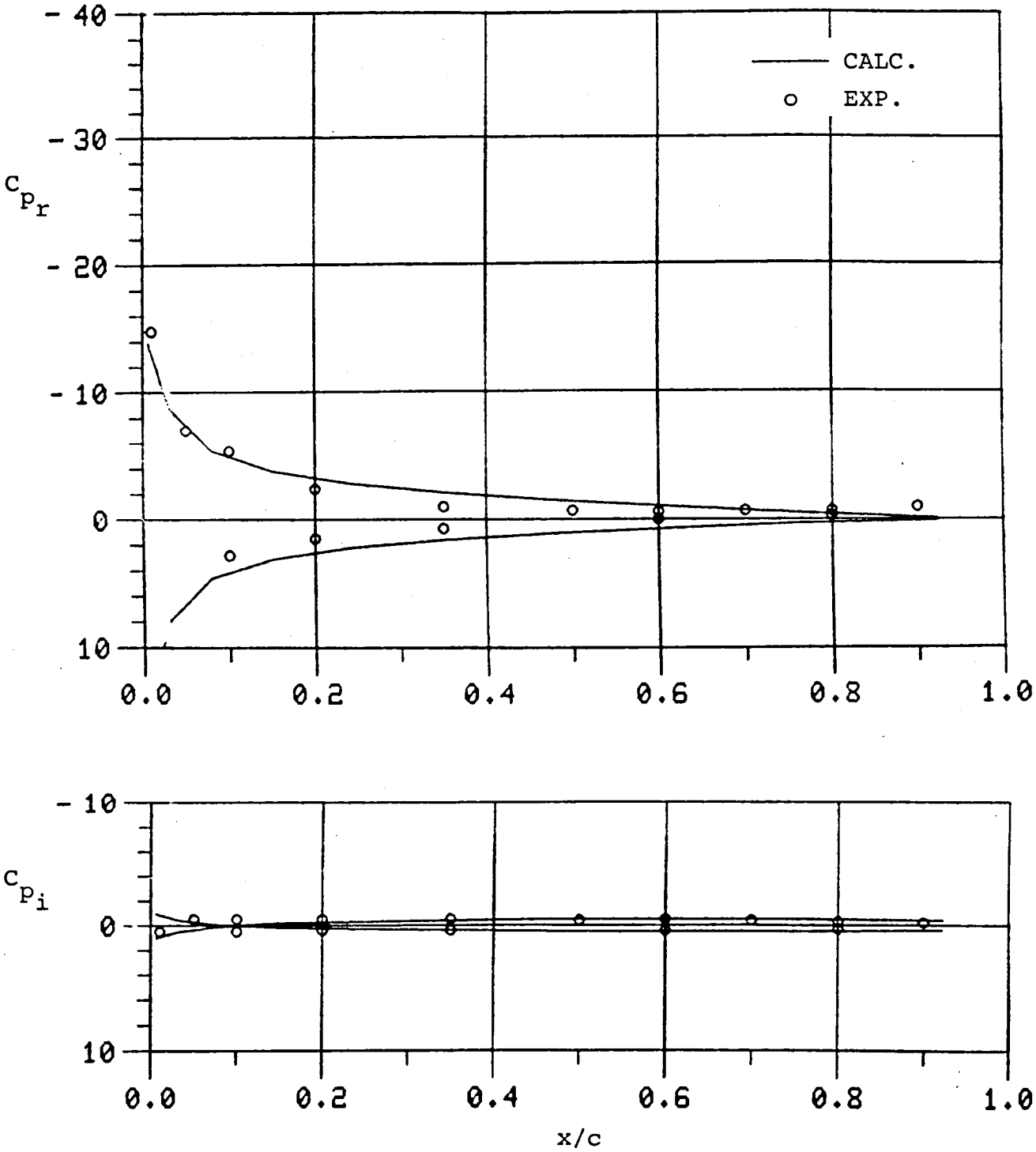

Figure 14(c). Comparison of Chordwise Pressure Distribution at y/s = 0.95 between Computed (VSAERO-H) and DFVLR Test, Tapered Tip (α_o = 12°, α_i = 0.703°, ω = 0.2).

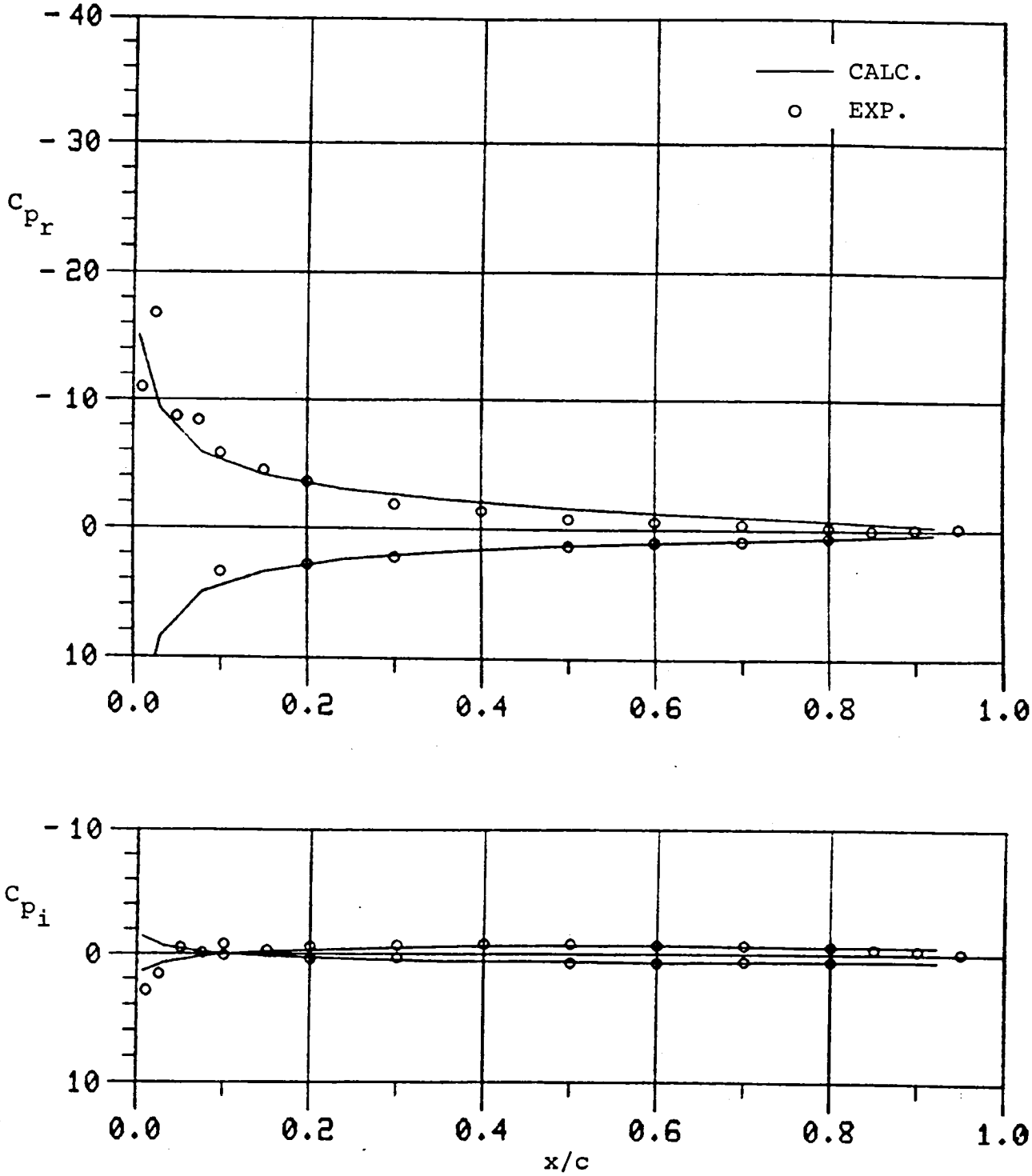

Figure 15(a). Comparison of Chordwise Pressure Distribution at y/s = 0.25 between Computed (VSAERO-H) and DFVLR Test, Tapered Tip (α_o = 12°, α_i = 0.703°, ω = 0.2).

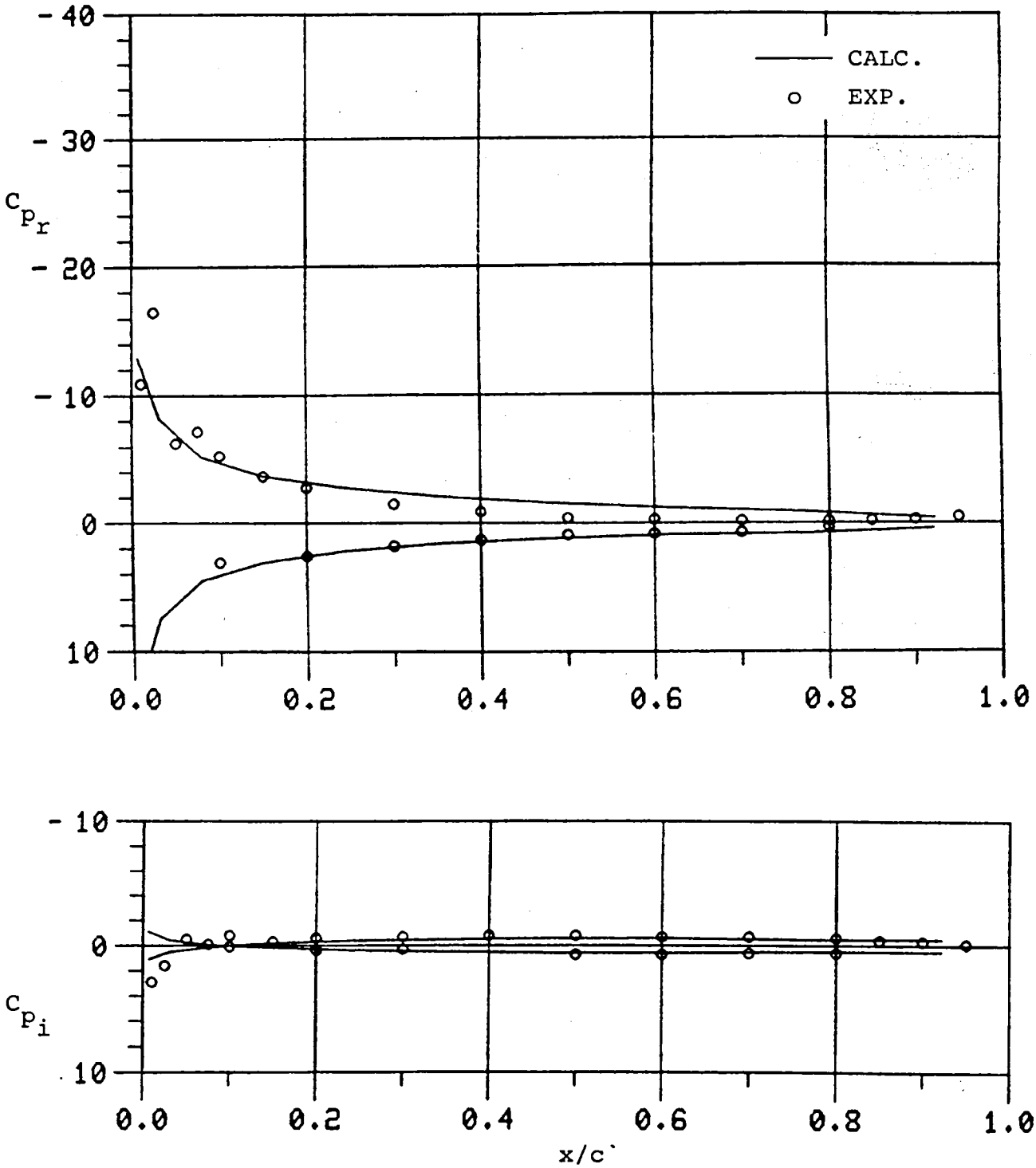

Figure 15(b). Comparison of Chordwise Pressure Distribution at y/s = 0.80 between Computed (VSAERO-H) and DFVLR Test, Tapered Tip (α_o = 12°, α_i = 0.703°, ω = 0.2).

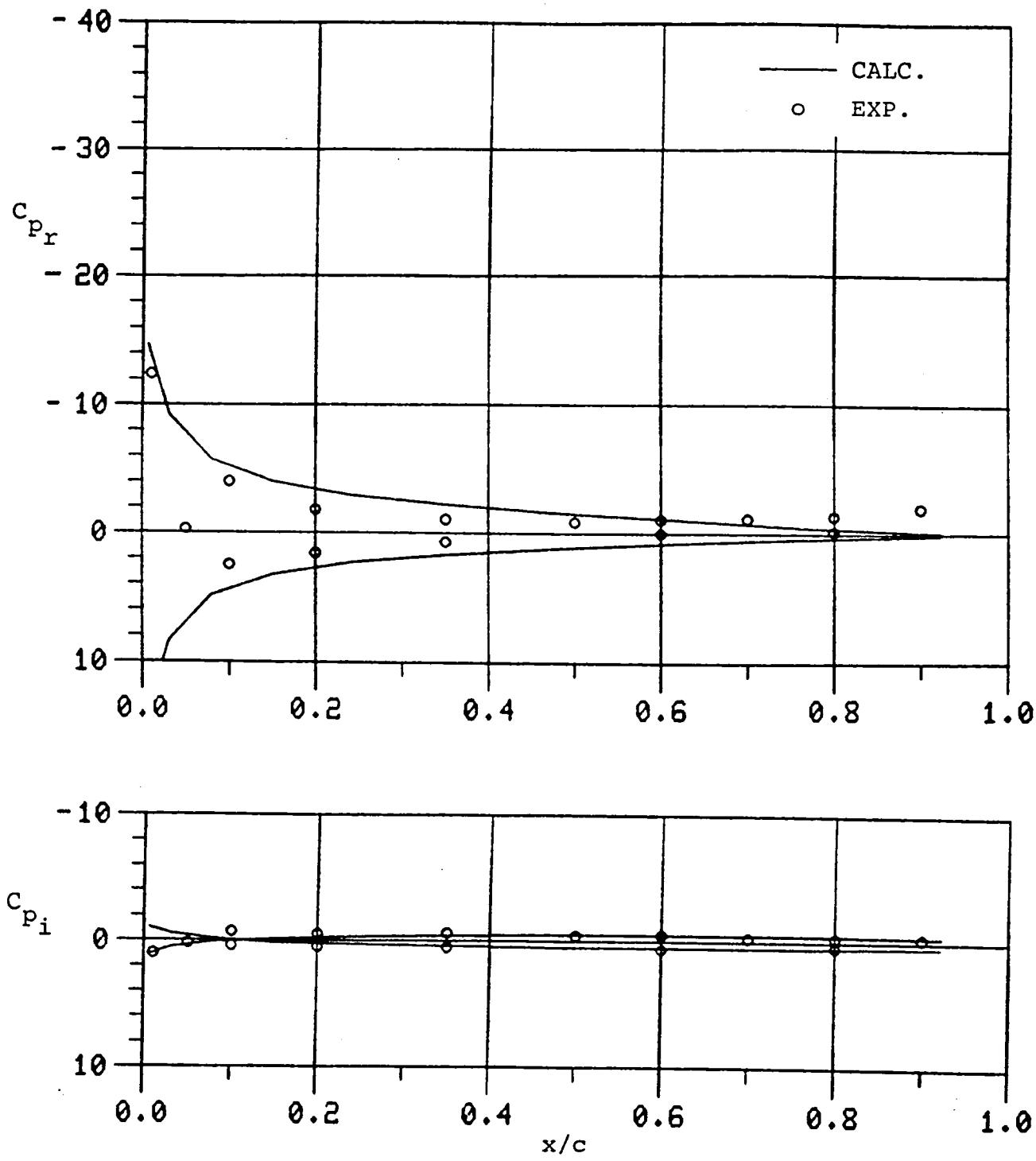

Figure 15(c). Comparison of Chordwise Pressure Distribution at y/s = 0.95 between Computed (VSAERO-H) and DFVLR Test, Tapered Tip (α_o = 12°, α_i = 0.703°, ω = 0.2).

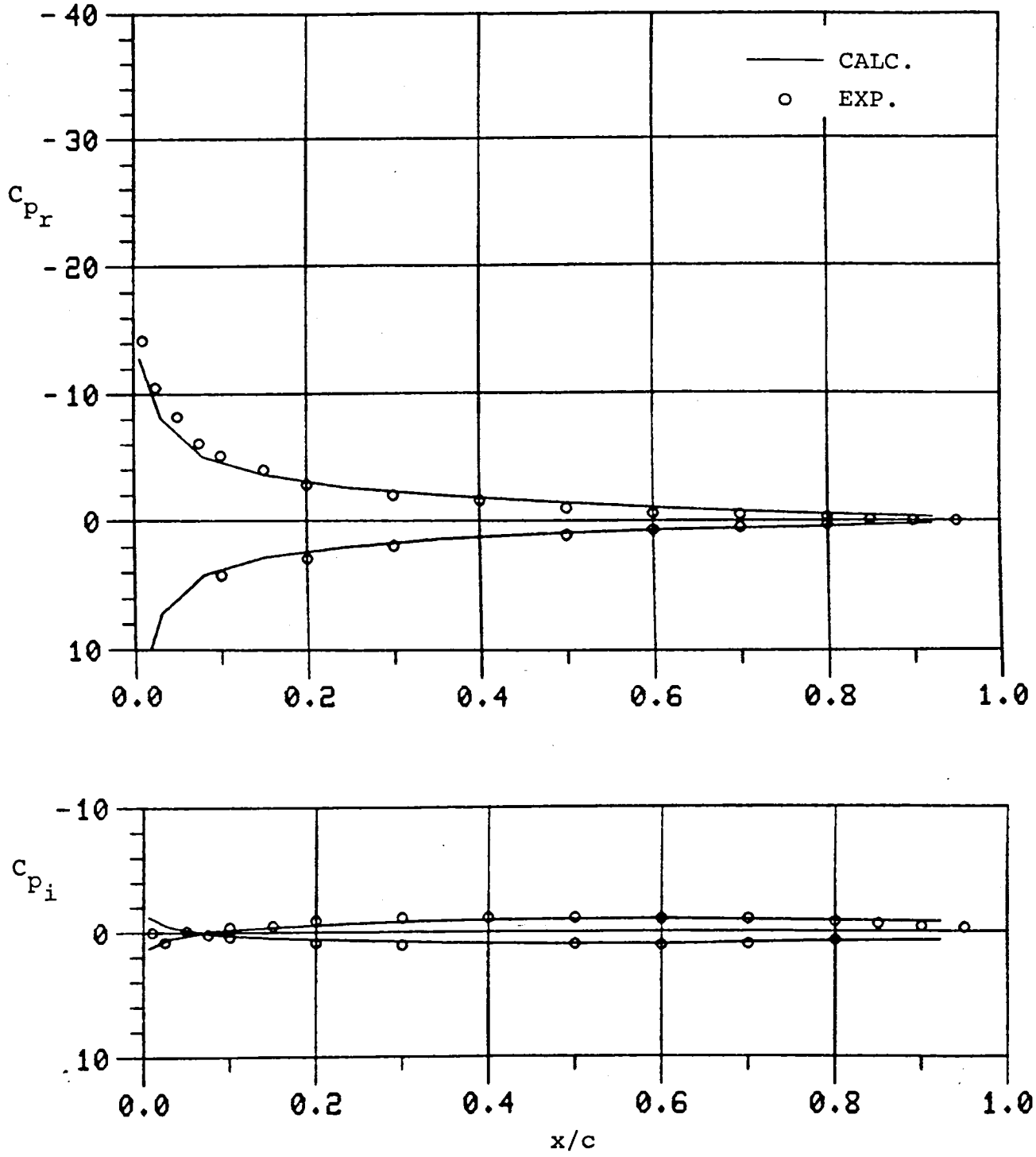

Figure 16(a). Comparison of Chordwise Pressure Distribution at y/s = 0.25 between Computed (VSAERO-H) and DFVLR Test, Tapered Tip (α_o = 4°, α_i = 0.705°, ω = 0.3).

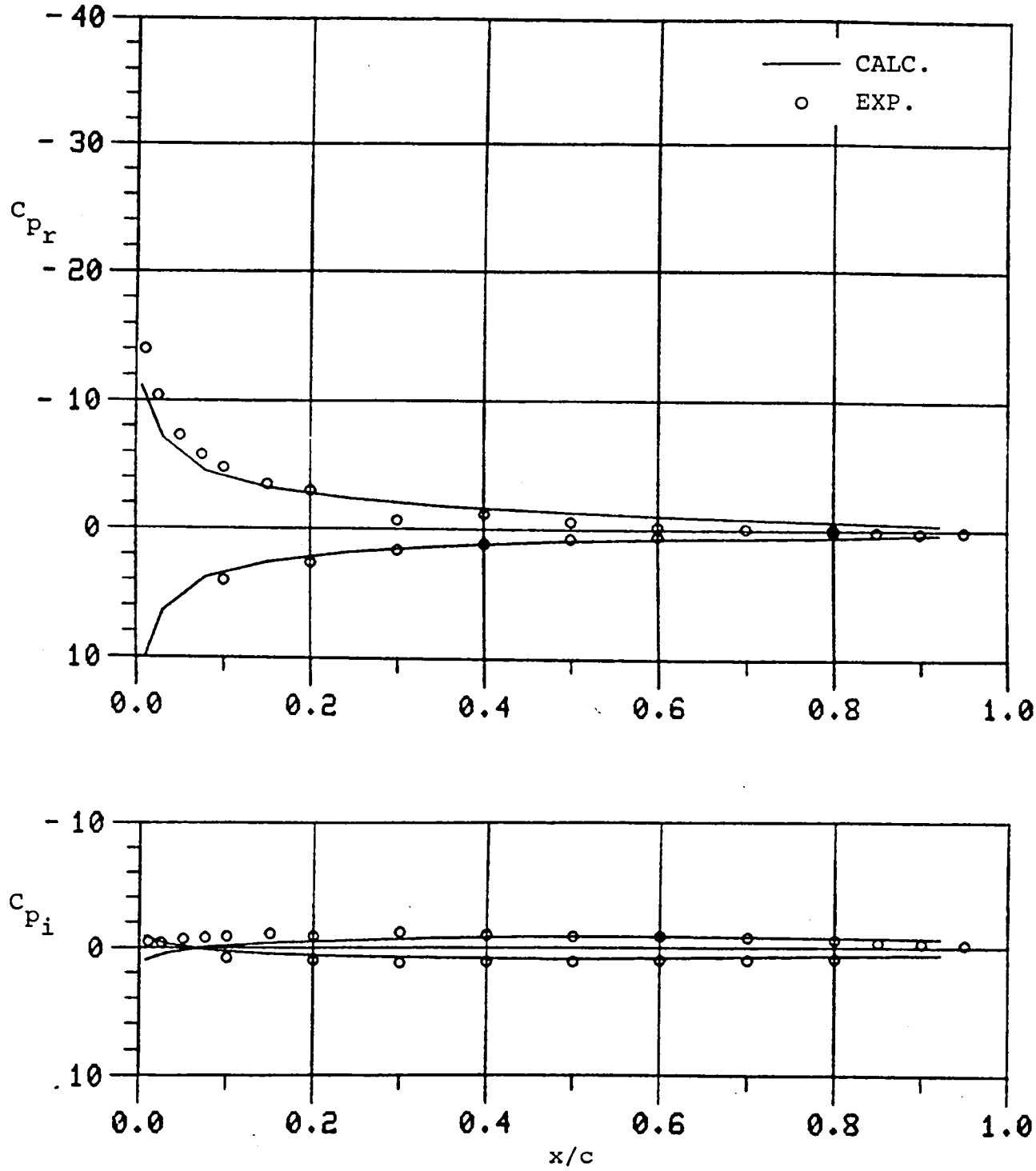

Figure 16(b). Comparison of Chordwise Pressure Distribution at y/s = 0.80 between Computed (VSAERO-H) and DFVLR Test, Tapered Tip (α_o = 4°, α_i = 0.705°, ω = 0.3).

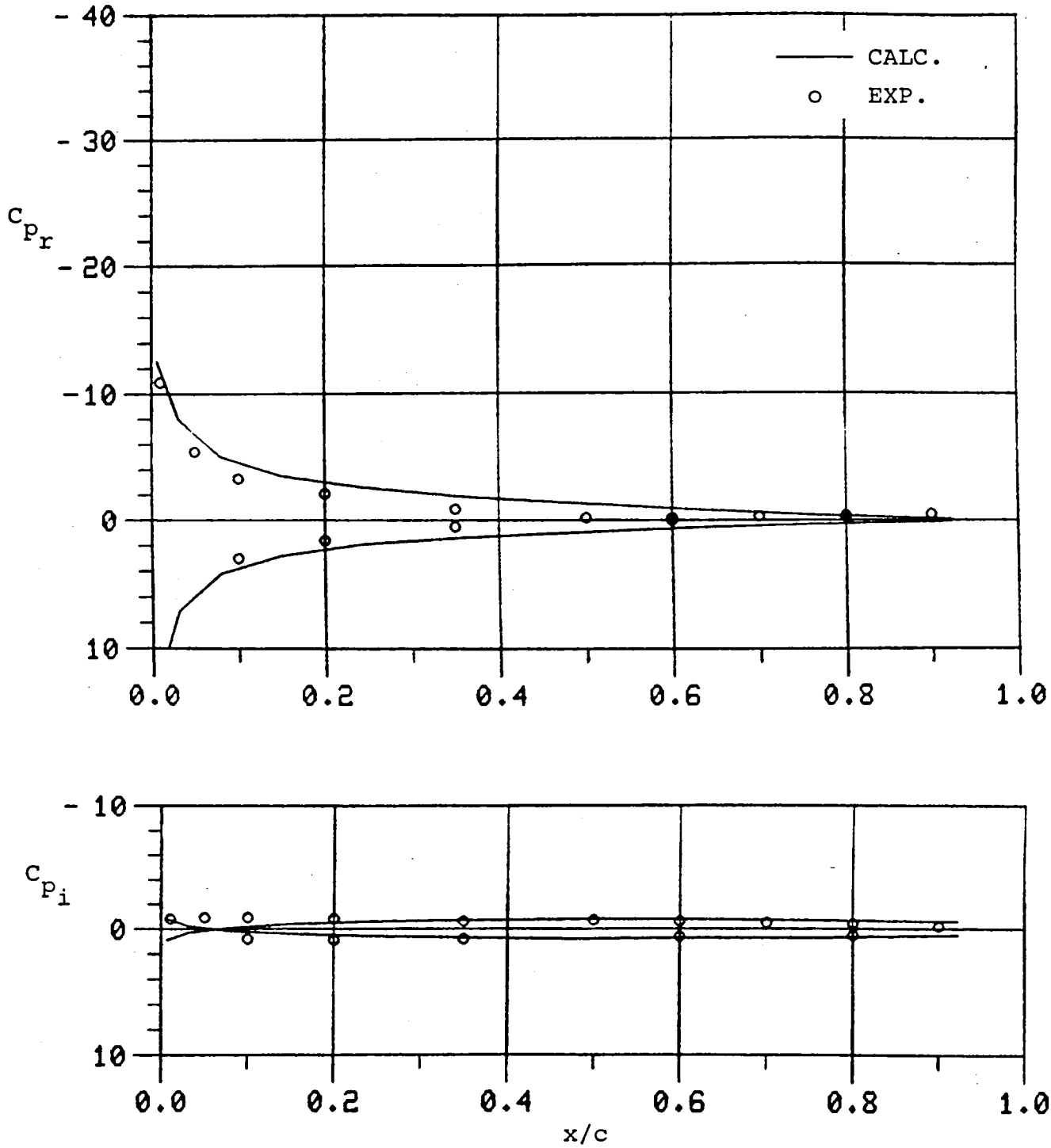

Figure 16(c). Comparison of Chordwise Pressure Distribution at y/s = 0.95 between Computed (VSAERO-H) and DFVLR Test, Tapered Tip (α_o = 4°, α_i = 0.705°, ω = 0.3).

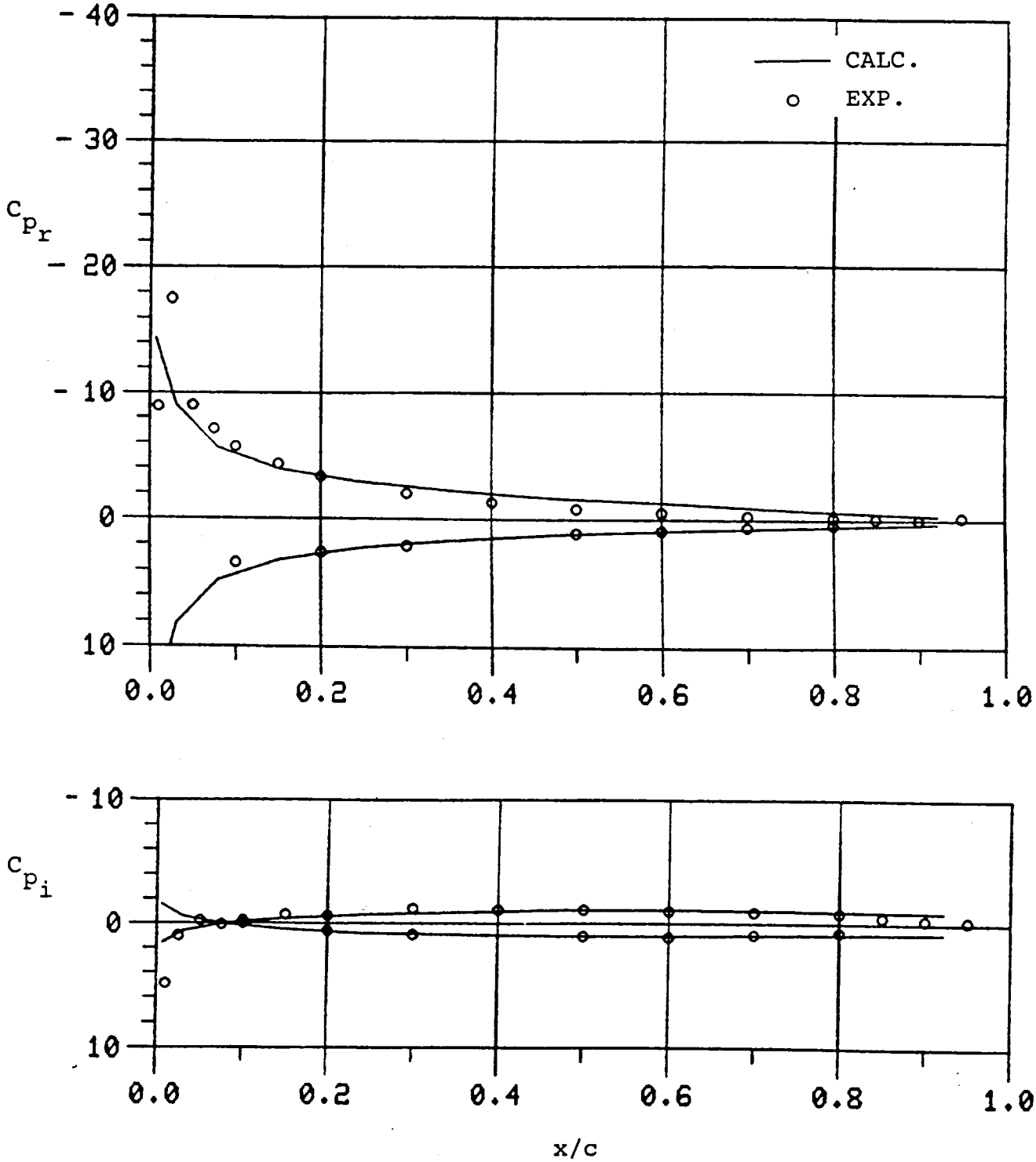

Figure 17(a). Comparison of Chordwise Pressure Distribution at y/s = 0.25 between Computed (VSAERO-H) and DFVLR Test, Tapered Tip (α_o = 12°, α_i = 0.701°, ω = 0.3).

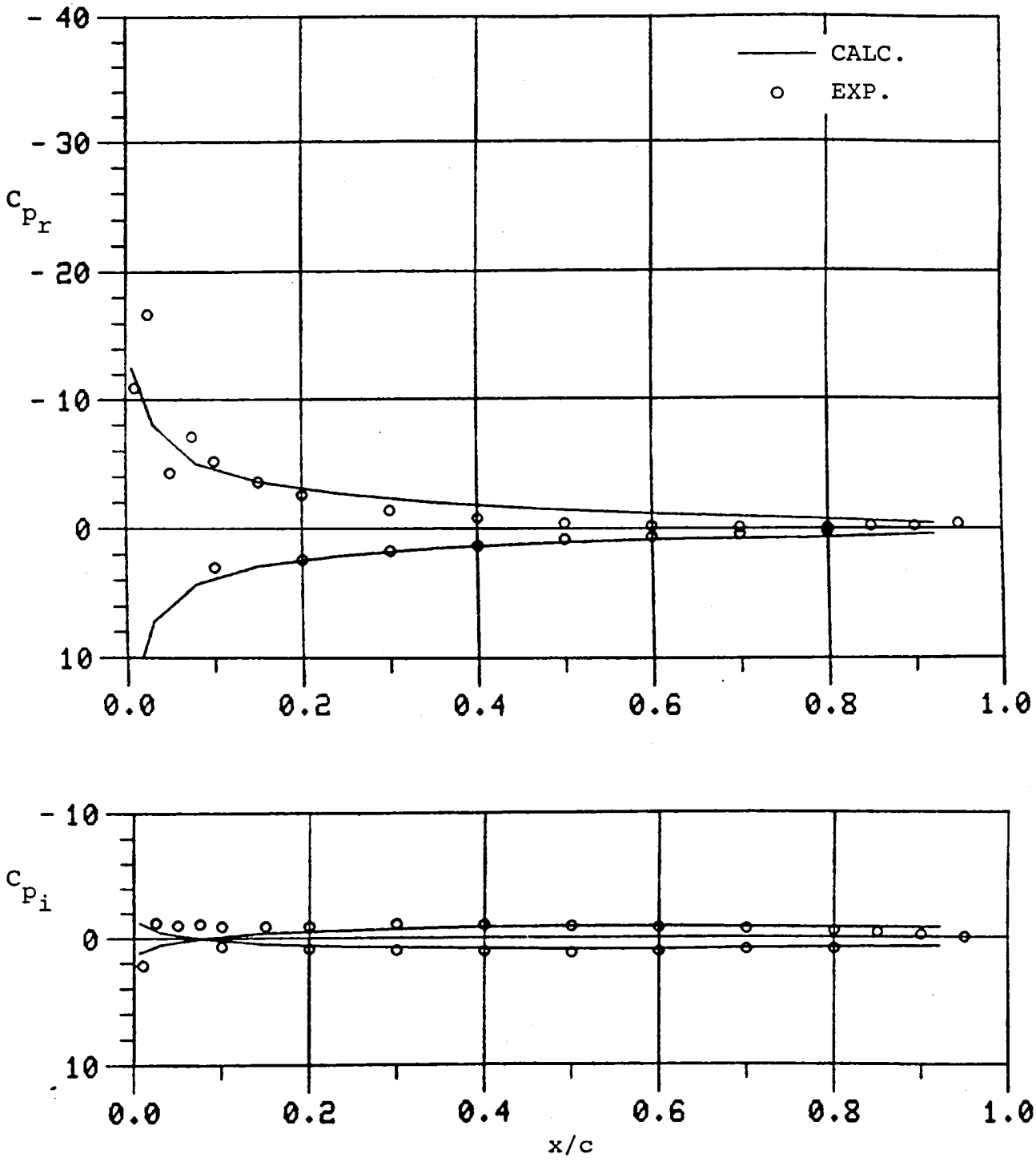

Figure 17(b). Comparison of Chordwise Pressure Distribution at y/s = 0.80 between Computed (VSAERO-H) and DFVLR Test, Tapered Tip (α_o = 12°, α_i = 0.701°, ω = 0.3).

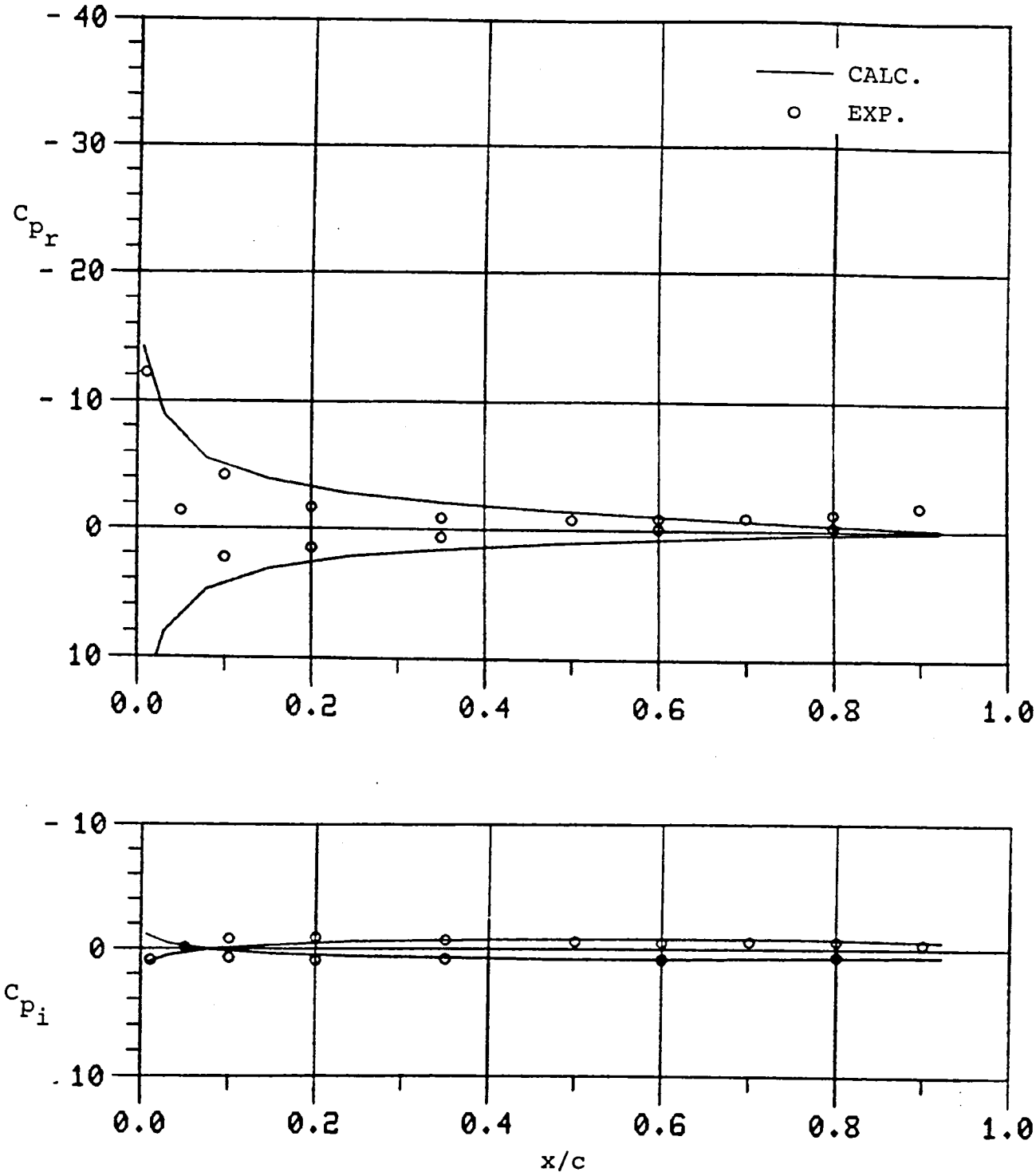

Figure 17(c). Comparison of Chordwise Pressure Distribution at y/s = 0.95 between Computed (VSAERO-H) and DFVLR Test, Tapered Tip (α_o = 12°, α_i = 0.701°, ω = 0.3).

5.0 OGEE TIP

VSAERO-H was used to compute several cases for an ogee tip wing. The following cases of comparison between the computed and the DFVLR experimental pressure distribution are presented:

Figure No.	α_o (degrees)	α_i (degrees)	ω
18	0	0.707	0.2
19	12	0.717	0.2
20	4	0.710	0.3
21	12	0.710	0.3

Table 3. Comparison between Computed and DFVLR Experimental Pressure Distribution for the Ogee Tip.

The cases included in this section cover the range of 0 to 12o angle of attack steady) and the reduced frequencies of 0.2 and 0.3. For each case the chordwise pressure distribution at three spanwise stations, y/s = 0.39, 0.85 and 0.99, for computed (VSAERO-H) and DFVLR test results is compared. In all cases investigated, the comparison is fair.

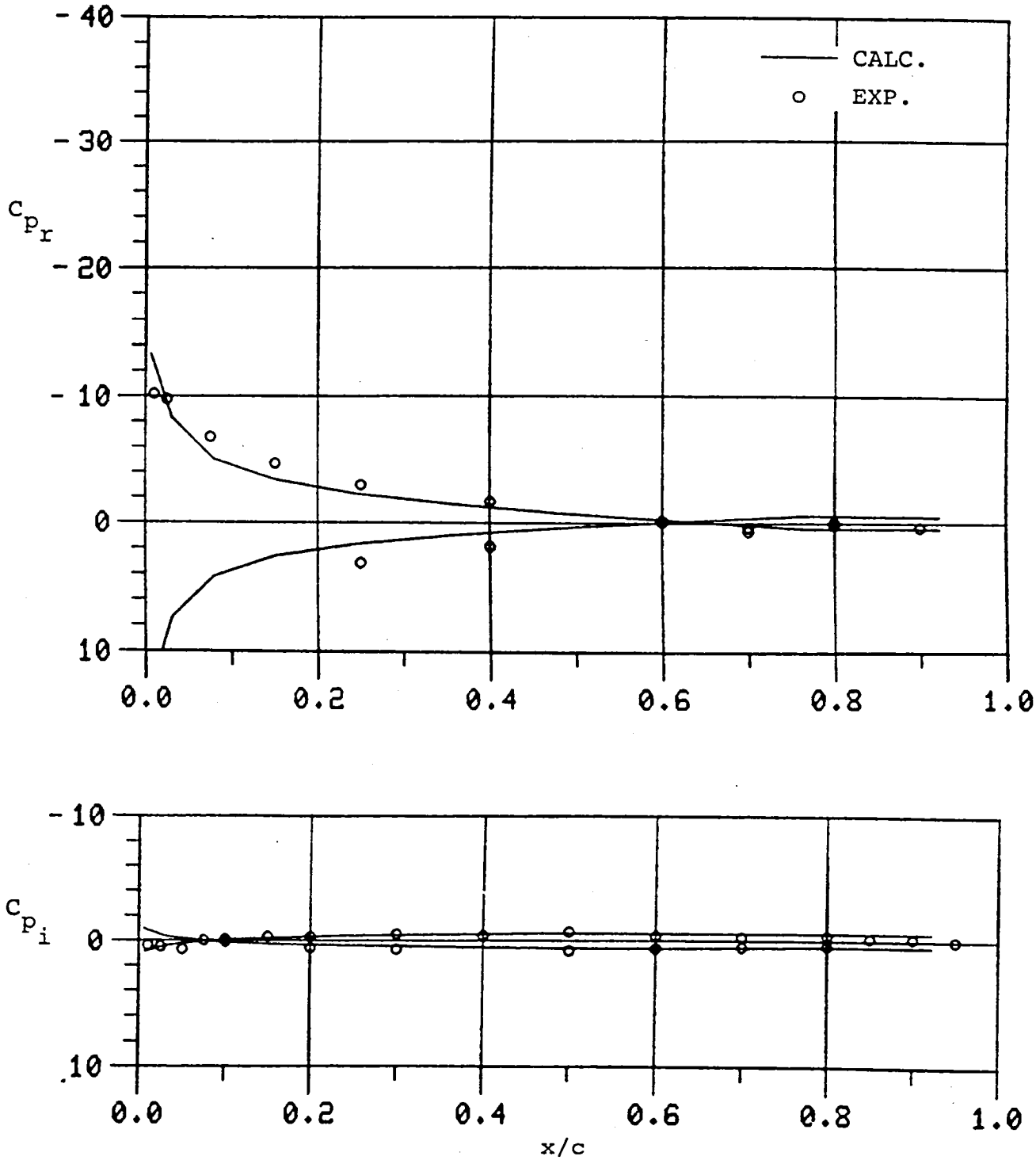

Figure 18(a). Comparison of Chordwise Pressure Distribution at y/s = 0.39 between Computed (VSAERO-H) and DFVLR Test, Ogee Tip (α_o = 0°, α_i = 0.707°, α = 0.2).

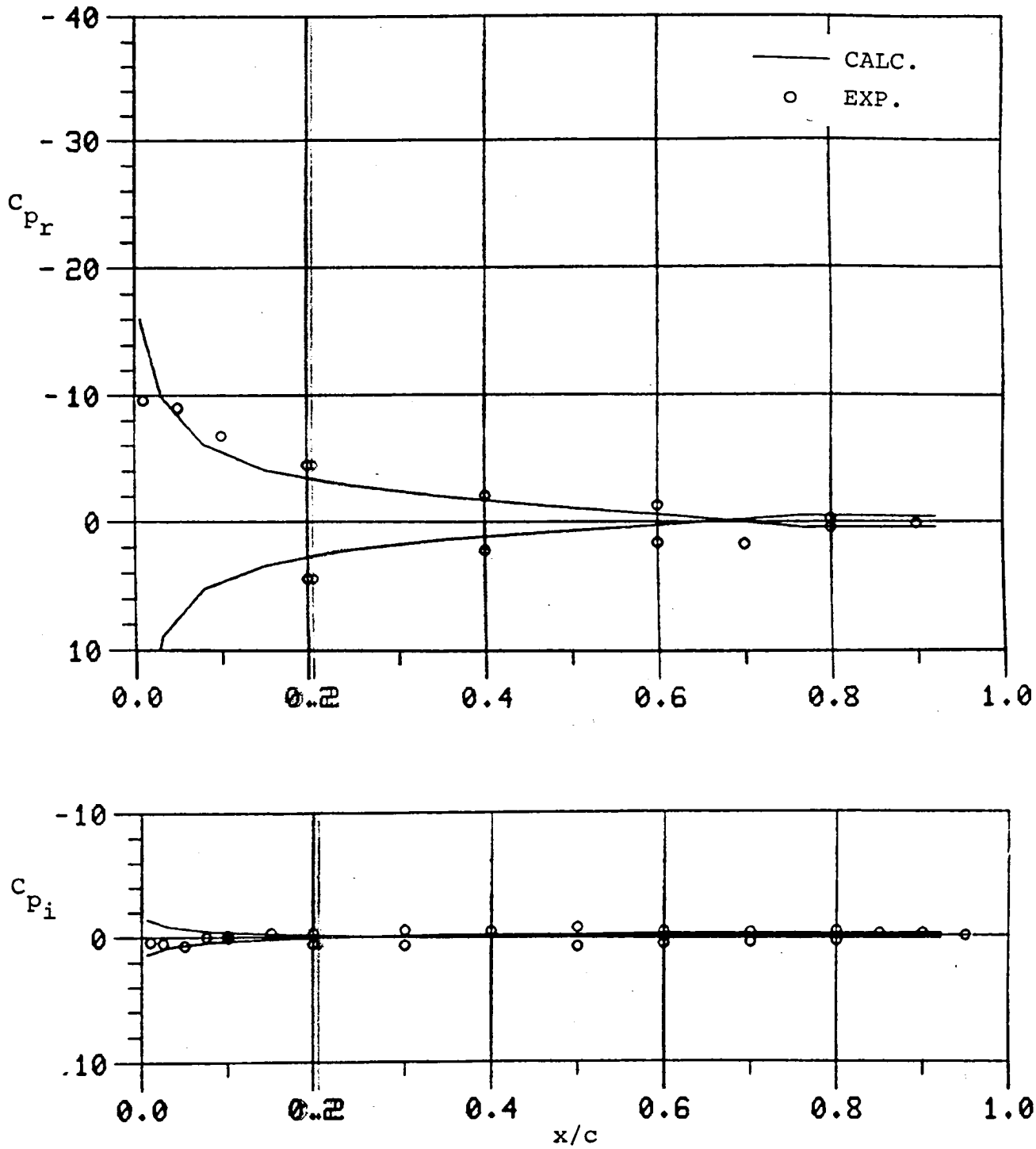

Figure 18(b). Comparison of Chordwise Pressure Distribution at y/s = 0.85 between Computed (VSAERO-H) and DFVLR Test, Ogee Tip (α_o = 0°, α_i = 0.707°, ω = 0.2).

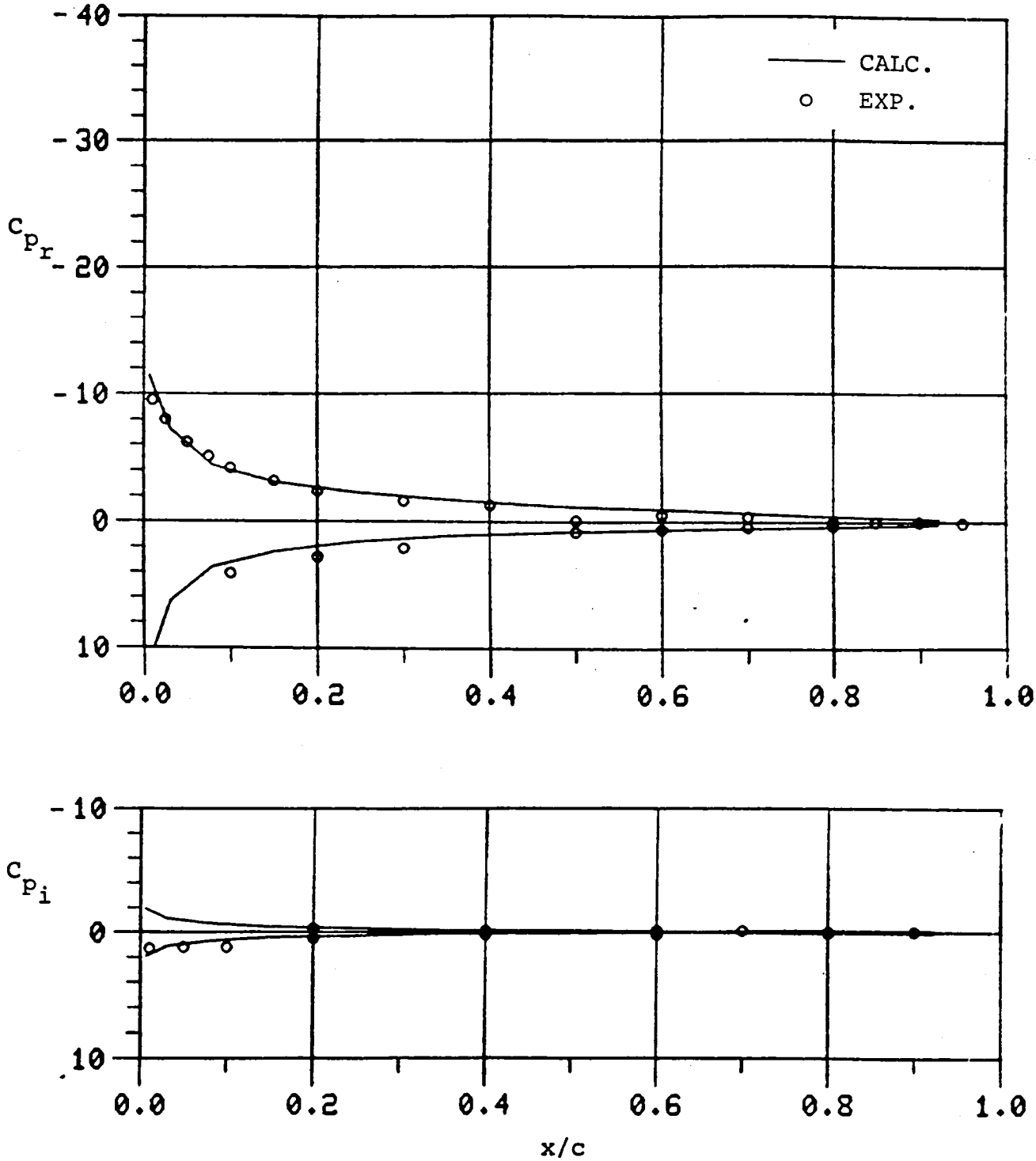

Figure 18(c). Comparison of Chordwise Pressure Distribution at y/s = 0.99 between Computed (VSAERO-H) and DFVLR Test, Ogee Tip (α_o = 0°, α_i = 0.707°, ω = 0.3).

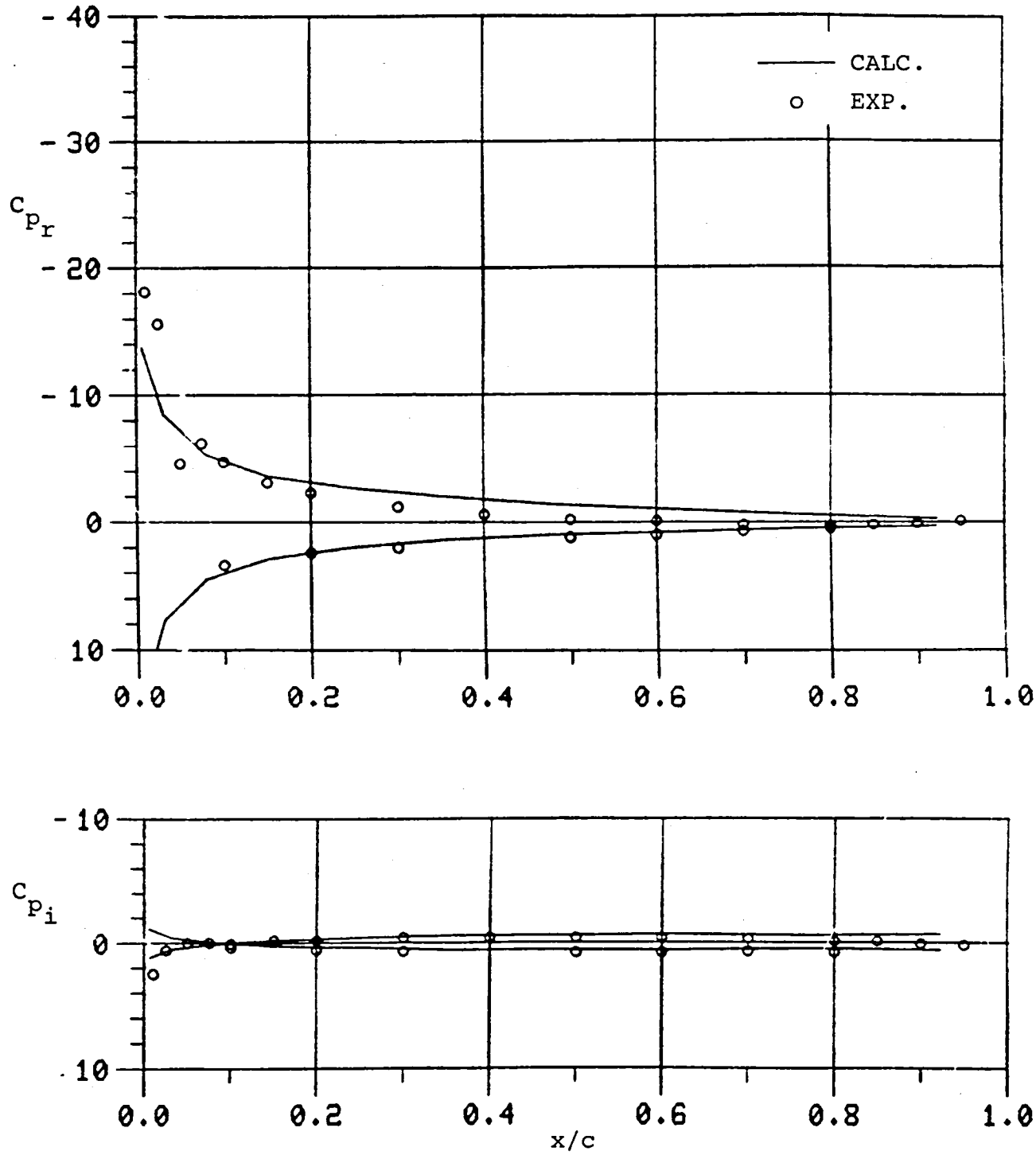

Figure 19(a). Comparison of Chordwise Pressure Distribution at y/s = 0.39 between Computed (VSAERO-H) and DFVLR Test, Ogee Tip (α_o = 12°, α_i = 0.717°, ω = 0.2).

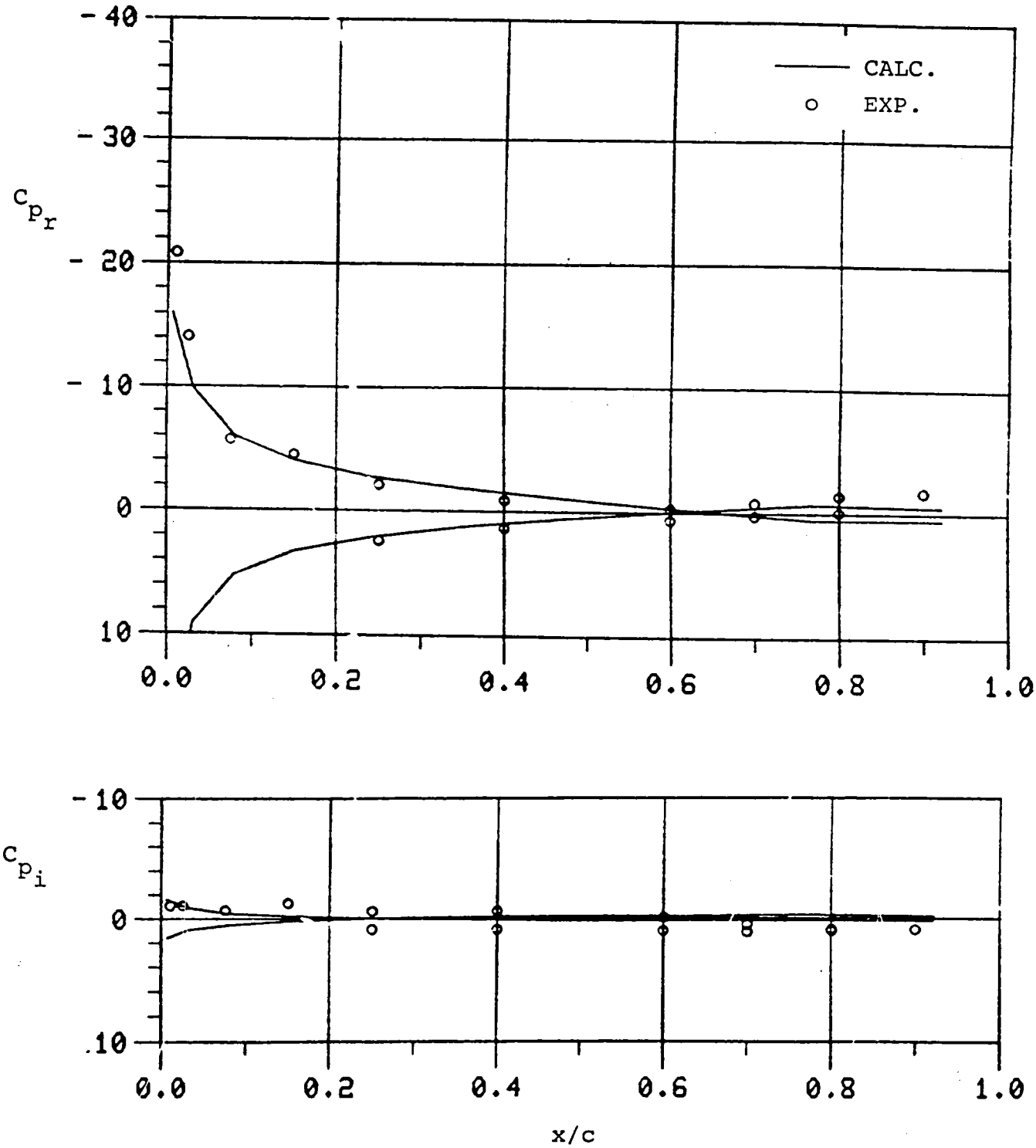

Figure 19(b). Comparison of Chordwise Pressure Distribution at y/s = 0.85 between Computed (VSAERO-H) and DFVLR Test, Ogee Tip (α_o = 12°, α_i = 0.717°, ω = 0.2).

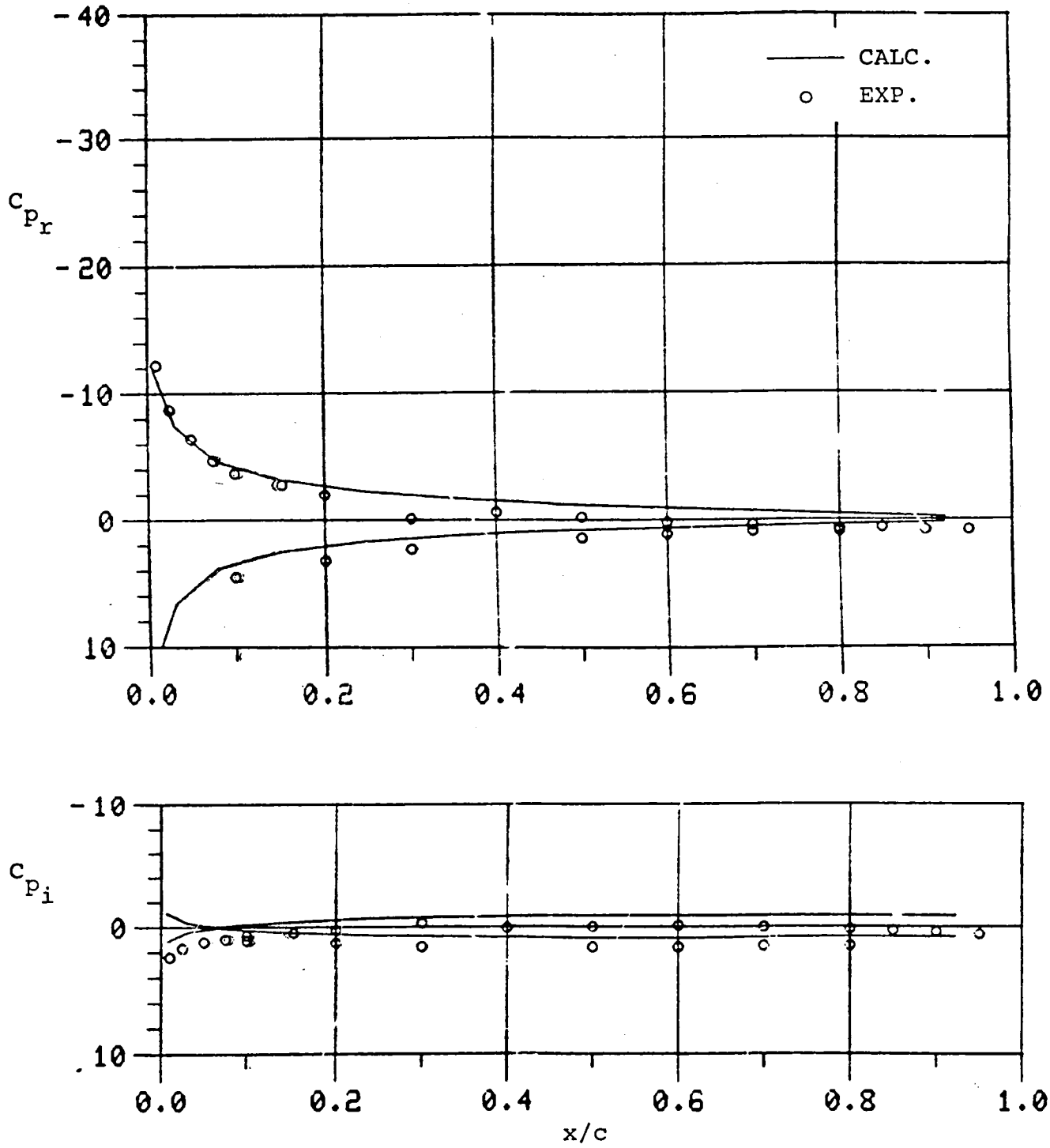

Figure 20(a). Comparison of Chordwise Pressure Distribution at y/s = 0.39 between Computed (VSAERO-H) and DFVLR Test, Ogee Tip (α_o = 4°, α_i = 0.710°, ω = 0.3).

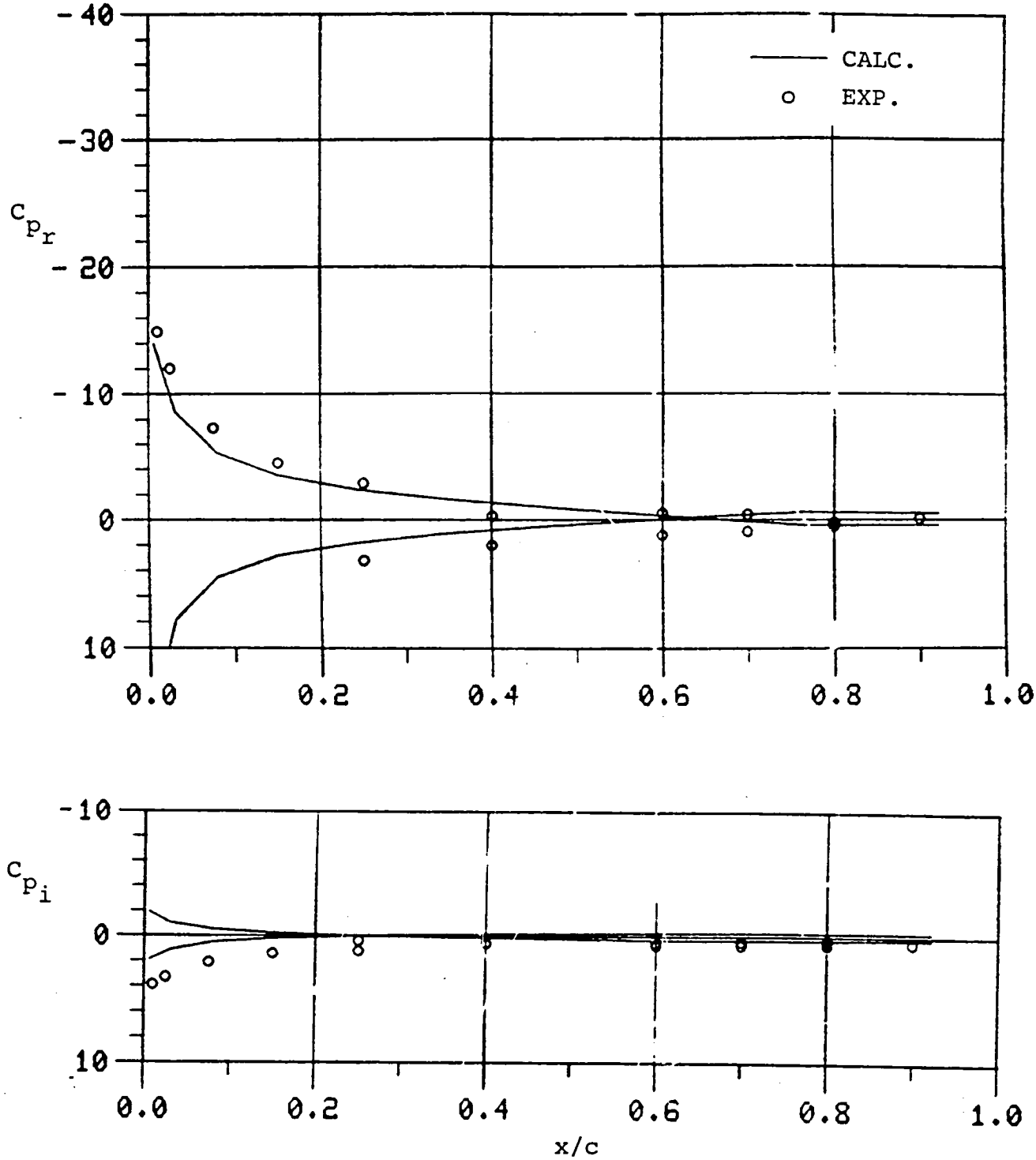

Figure 20(b). Comparison of Chordwise Pressure Distribution at y/s = 0.85 between Computed (VSAERO-H) and DFVLR Test, Ogee Tip (α_o = 4°, α_i = 0.710°, ω = 0.3).

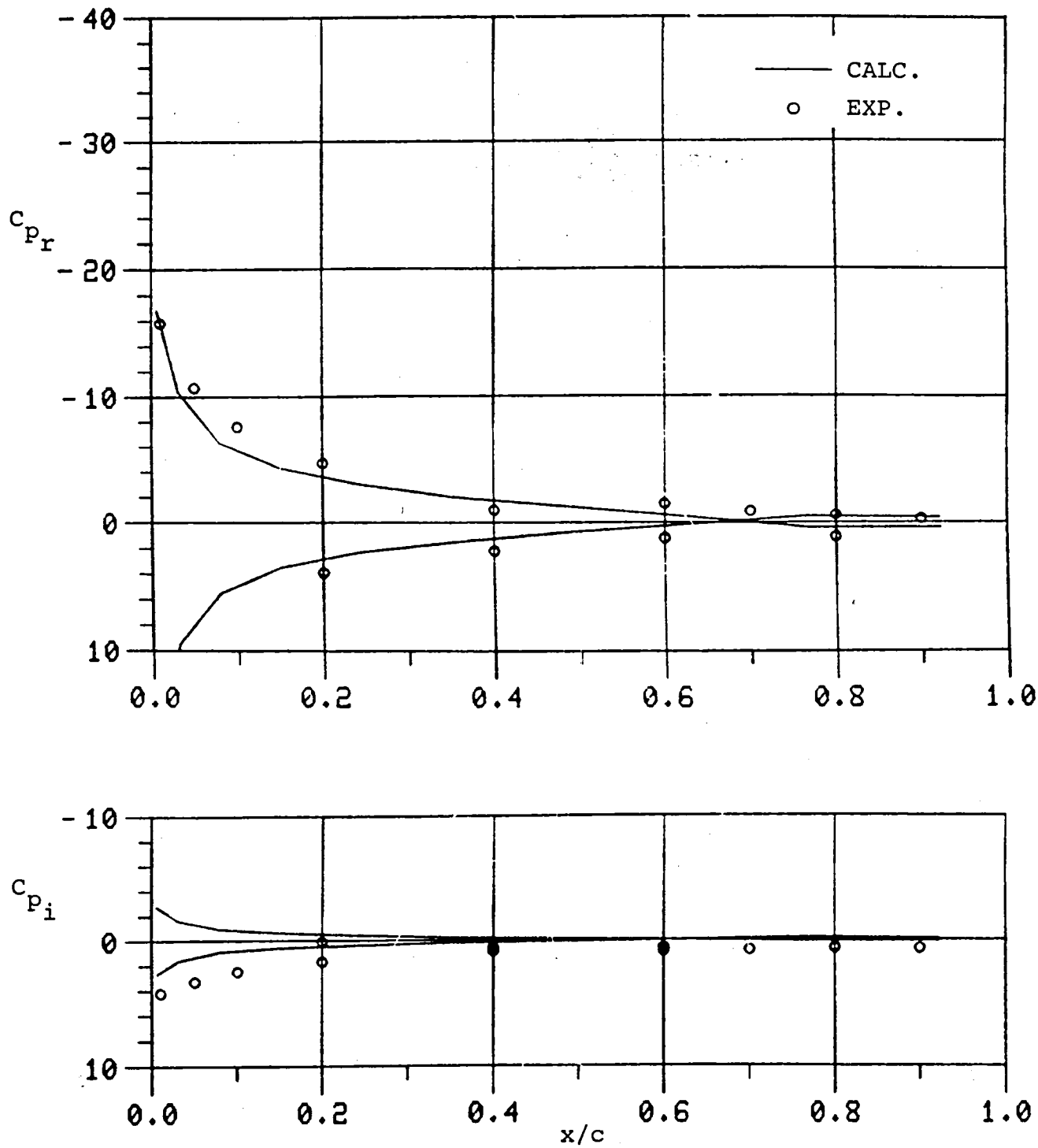

Figure 20(c). Comparison of Chordwise Pressure Distribution at y/s = 0.99 between Computed (VSAERO-H) and DFVLR Test, Ogee Tip (α_o = 4°, α_i = 0.710°, ω = 0.3).

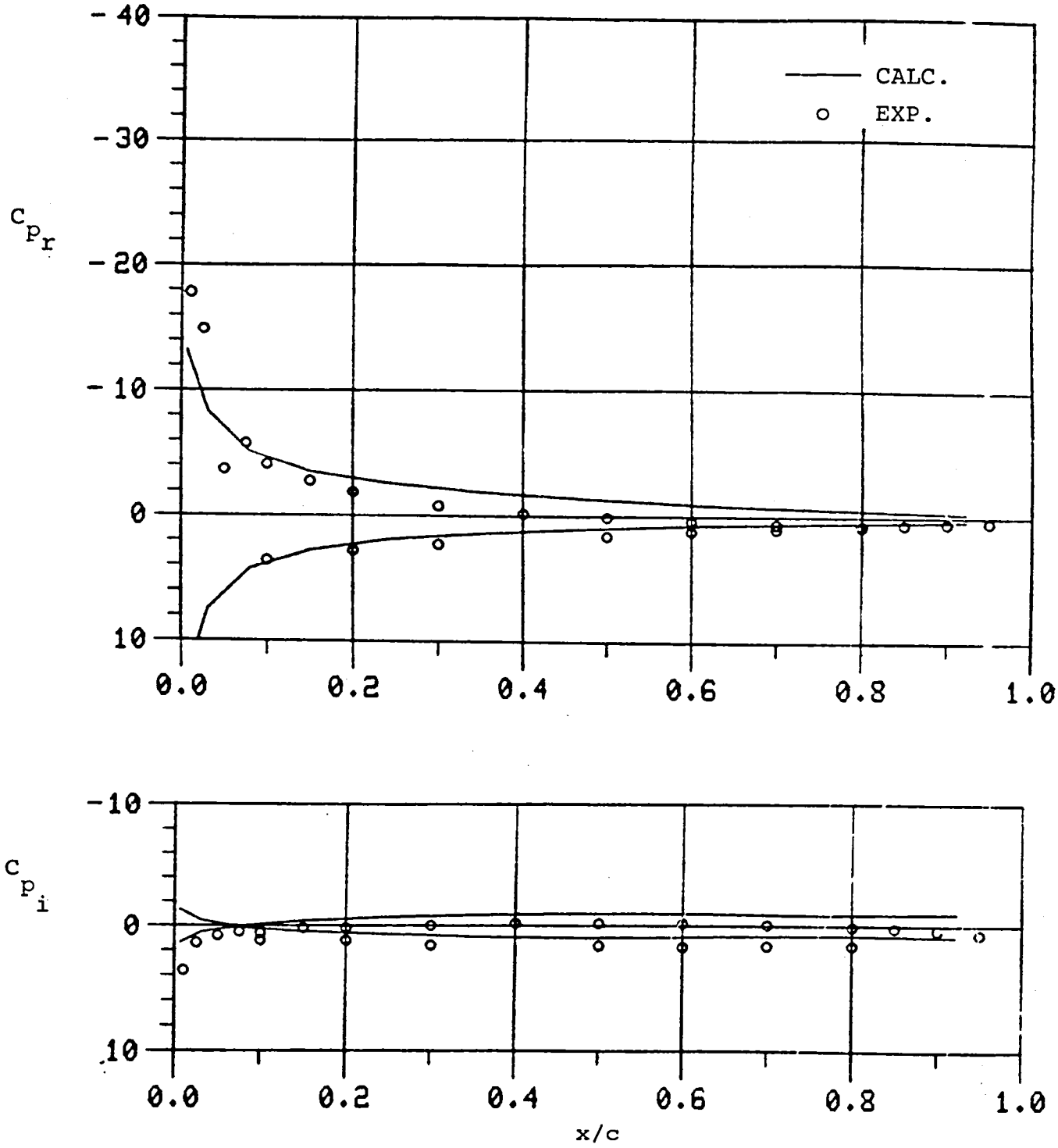

Figure 21(a). Comparison of Chordwise Pressure Distribution at y/s = 0.39 between Computed (VSAERO-H) and DFVLR Test, Ogee Tip (α_o = 12°, α_i = 0.710°, ω = 0.3).

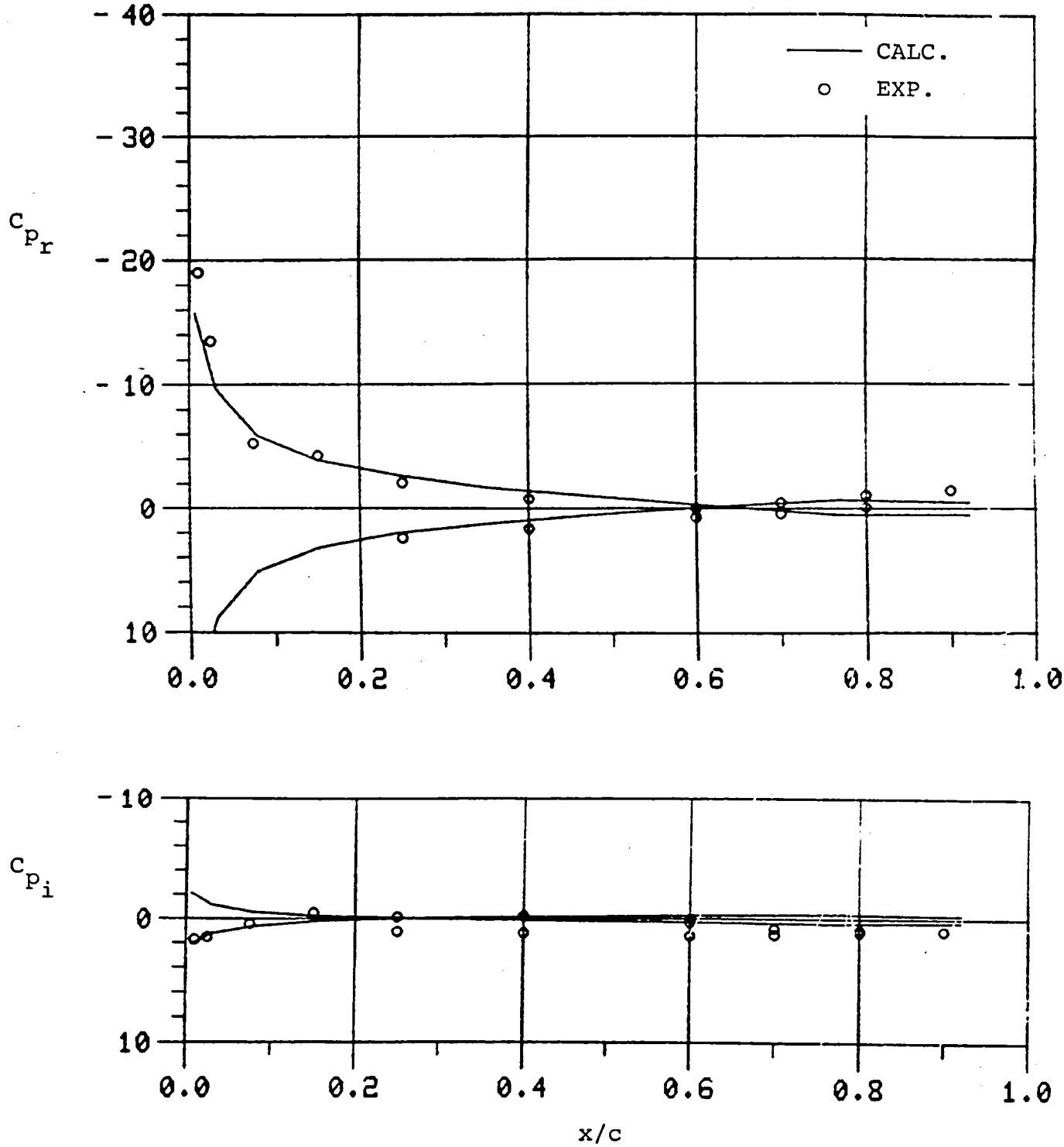

Figure 20(b). Comparison of Chordwise Pressure Distribution at y/s = 0.85 between Computed (VSAERO-H) and DFVLR Test, Ogee Tip (α_o = 12°, α_i = 0.710°, ω = 0.3).

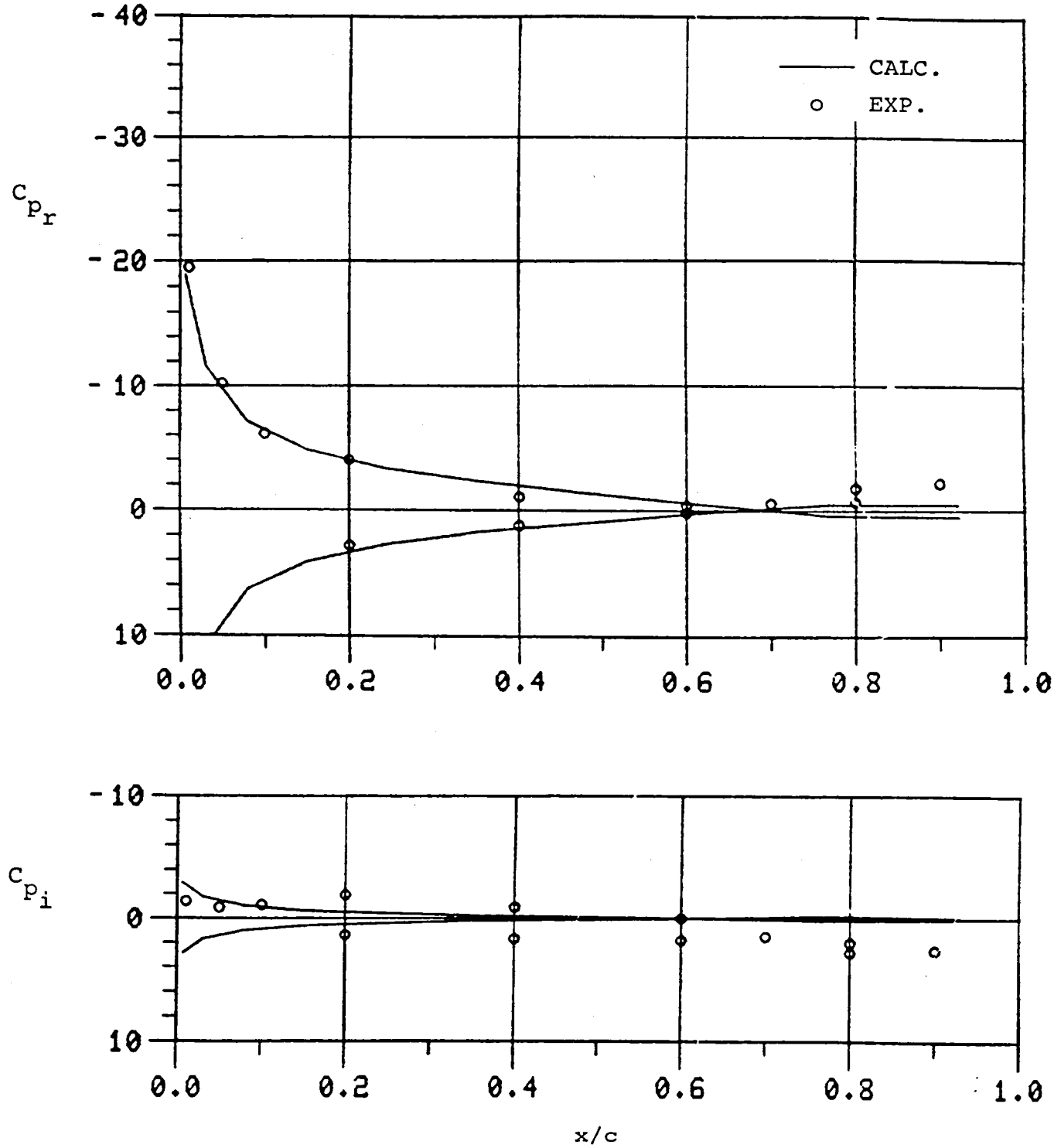

Figure 20(c). Comparison of Chordwise Pressure Distribution at y/s = 0.99 between Computed (VSAERO-H) and DFVLR Test, Ogee Tip (α_o = 12°, α_i = 0.710°, ω = 0.3).

6.0 CONCLUSIONS

A comparison between the computed (VSAERO-TS and VSAERO-H) and DFVLR test results for chordwise pressure distributions for rectangular, swept, taper and ogee blade tips is presented in this report. A complete discussion on the theory, limitations and the convergence characteristics of the VSAERO-TS and VSAERO-H codes are presented in a separate theory document.

A wide range of angles of attack (mean) from 0 to 12 degrees and reduced frequencies of 0.1, 0.2 and 0.3 are covered in this report. Also, the comparison includes several spanwise stations. For the most part the comparison between the theory and experiment is very good for the range of conditions covered; however, the time-stepping calculations (VSAERO-TS) showed a sensitivity to the relative wake-shedding panel size and time step size. Results from this program were not, therefore, presented for the tapered and ogee tip cases. Although some good comparisons were obtained for these cases, the number of time steps required was impractically large. Ways of alleviating this sensitivity are being examined. The harmonic wake calculations (VSAERO-H) were good over the full range of conditions considered.

7.0 REFERENCES

1. Maskew, B., "Influence of Rotor Blade Tip Shape on Tip Vortex Shedding--An Unsteady Inviscid Analysis", Paper 80-6 in Proc. 36th Annual Forum of Am. Hel. Soc., May 1980.

2. Maskew, B., "Prediction of Subsonic Aerodynamic Characteristics: A Case for Low-Order Panel Methods", J. Aircraft, Vol. 19, No. 2, February 1982.

3. Maskew, B. Rao, B.M. and Dvorak, F.A., "Prediction of Aerodynamic Characteristics for Wings with Extensive Separations", Paper No. 31 in Computation of Viscous-Inviscid Interactions, AGARD CPP-291, September 1980.

4. Clark, D.R., Maskew, B. and Dvorak, F.A., "The Application of a Second Generation Low-Order Panel Method, Program VSAERO, to Powerplant Installation Studies", Paper 84-0122, Presented at AIAA Aerospace Sciences Meeting, Reno, Nevada, January 1984.

5. Maskew, B. and Rao, B.M., "Unsteady Analysis of Rotor Blade Tip Flow", NASA CR-3868, 1985.

1. Report No.	2. Government Accession No.	3. Recipient's Catalog No.
NASA CR-172506		

4. Title and Subtitle	5. Report Date
INVISCID ANALYSIS OF UNSTEADY BLADE TIP FLOW CORRELATION STUDIES	February 1985
	6. Performing Organization Code

7. Author(s)	8. Performing Organization Report No.
B. M. Rao and B. Maskew	AMI Report 8409
	10. Work Unit No.

9. Performing Organization Name and Address	11. Contract or Grant No.
Analytical Methods, Inc. 2047 - 152nd Avenue N.E. Redmond, WA 98052	NAS1-15472
	13. Type of Report and Period Covered
12. Sponsoring Agency Name and Address	Contractor Report
NASA Langley Research Center Hampton, VA 23665	14. Sponsoring Agency Code

15. Supplementary Notes

Final Report

16. Abstract

Two computer programs, VSAERO-TS and VSAERO-H, were used for computing the unsteady subsonic aerodynamic characteristics of arbitrarily shaped wings oscillating in pitch. Program VSAERO-TS is a time-stepping analysis capable of treating large amplitude motions while program VSAERO-H uses harmonic wake and small amplitude assumptions.

A comparison between the computed (VSAERO-TS and VSAERO-H) and DFVLR test results for chordwise pressure distributions for rectangular, swept, taper and ogee blade tips is presented in this report. A complete discussion on the theory, limitations and the convergence characteristics of the VSAERO-TS and VSAERO-H codes are presented in NASA CR-3868.

A wide range of angles of attack (mean) from 0° to 12° and reduced frequencies of 0.1, 0.2 and 0.3 are covered in this report. Also, the comparison includes several spanwise stations. For the most part, the comparison between the theory and experiment is very good for the range of conditions covered; however, the time-stepping calculations (VSAERO-TS) showed a sensitivity to the relative wake-shedding panel size and time step size. The harmonic wake calculations (VSAERO-H) were good over the full range of conditions considered.

17. Key Words (Suggested by Author(s))	18. Distribution Statement
Unsteady Flows Subsonic Aerodynamics Blade Tip Planforms Time-stepping Computations Harmonic Analysis	Unclassified; Unlimited.

19. Security Classif. (of this report)	20. Security Classif. (of this page)	21. No. of Pages	22. Price
Unclassified	Unclassified	59	

For sale by the National Technical Information Service, Springfield, Virginia 22161